MOLECULAR MECHANISMS OF CYTOTOXICITY INDUCED BY RIBOSOME-INACTIVATING PROTEINS IN MAMMALIAN CELLS

By

JU-SHUN CHENG

A thesis submitted to the

Graduate School-New Brunswick

Rutgers, The State University of New Jersey

in partial fulfillment of the requirements

for the degree of

Master of Science

Graduate Program in Endocrinology and Animal Biosciences

written under the direction of

Wendie Cohick

and approved by

_____

_____

_____

New Brunswick, New Jersey

October, 2010

ABSTRACT OF THE THESIS

MOLECULAR MECHANISMS OF CYTOTOXICITY INDUCED BY

RIBOSOME-INACTIVATING PROTEINS IN MAMMALIAN CELLS

BY JU-SHUN CHENG

Thesis Director:

Dr. Wendie S. Cohick

Ribosome-inactivating proteins (RIP) represent a family of plant and bacterial toxins that inhibit protein synthesis and are cytotoxic to mammalian cells. Ricin is isolated from seeds of the castor bean plant and has potential as a weapon of bioterrorism. Shiga-like toxins (stx) are produced from enterohemorrahagic *Escherichia coli* strains, and contamination of food by stx represents a substantial public health threat. Both ricin and stx consist of A and B chains. The A-chain of each protein inactivates the ribosome by cleaving an adenine from the ribosomal RNA. The B-chain of ricin (RTB) binds to galactose binding sites on the cell surface while the pentameric B subunit of stx binds to the cell surface receptor, globotriaosylceramide to facilitate cell entry. While both ricin and stx inhibit protein synthesis and induce cell death, the molecular mechanisms that

underlie these effects are relatively unexplored. An ultimate goal of this research is to produce recombinant mutant ricin A-chain (RTA) proteins to study the role of protein synthesis inhibition in ricin-induced cytotoxicity. Therefore, we were interested in establishing a mammalian cell culture model that was sensitive to RTA alone. The cell line MAC-T, an immortalized, nontransformed epithelial cell line, was more sensitive than Vero cells and HeLa cells in terms of the time it took to induce caspase-3/7 activation. While ricin induced higher caspase-3/7 activity than RTA at lower concentrations (0.1 to 10 ng/ml), similar caspase activation was observed at concentrations of 0.1 μg/ml with either protein. Ribosome depurination, protein synthesis inhibition, and apoptosis were observed in MAC-T cells treated with RTA alone. RTA alone also induced JNK and p38 MAP kinase activation in a time- and concentration-dependent manner that preceded apoptosis. Inhibition of the JNK pathway by chemical inhibitors or small interfering RNA reduced RTA-induced apoptosis. In contrast, inhibition of the p38 MAP kinase pathway had little effect on RTA-induced apoptosis.

In summary, the major findings of this research are the establishment of the MAC-T cell line as a sensitive cell culture model for future study of ricin and the finding that the JNK pathway plays a major role in RTA-induced cytotoxicity.

DEDICATION

To My Parents

I dedicate this work to them, for their love and support

ACKNOWLEDGEMENTS

I would like to express my deepest appreciation to Dr. Wendie Cohick for accepting me as an advisee and for guiding me throughout my graduate work. She is not only an enthusiastic and positive advisor, but also the most influential person on my development and character in my life. I am grateful to her for her support and advice, and there is not a day when I don't.

I would like to thank my committee members, Drs. Carol Bagnell and Malcolm Watford for their advice and support. Words cannot phrase how humbled I am to learn from such intelligent and admirable teachers.

Special thanks to Dr. Amanda Jetzt for giving me numerous insightful advice. We worked together very closely on the ricin project, and I could not have done my research without her hard work and invaluable support.

Finally, thanks to my family for their love and support.

TABLE OF CONTENTS

LIST OF FIGURES

LIST OF ABBREVIATIONS

BSA	bovine serum albumin
DMEM-H	Dulbecco's Modified Eagle's Medium-high glucose
EF 2	elongation factor 2
ER	endoplasmic reticulum
ERK	extracellular signal-regulated kinase
FBS	fetal bovine serum
Gb3	globotriaosylceramide
HUS	hemolytic uremic syndrome
JNK	c-jun N-terminal kinase
L3Δ99	N-terminal fragment of yeast ribosomal protein L3
MAPK	mitogen-activated protein kinase
MEC	mammary epithelial cell
PAGE	polyacrylamide gel electrophoresis
PBS	phosphate buttered saline
PAP	pokeweed antiviral protein

PARP	poly (ADP-ribose) polymerase
PR	phenol red
PVDF	polyvinylidene fluoride
rRNA	ribosomal RNA
RIP	ribosome-inactivating protein
RTA	ricin-A-chain
RTB	ricin-B-chain
SAPK	stress-activated protein kinase
SDS	sodium dodecyl sulfate
Stx	Shiga-like toxin
TCA	trichloroacetic acid
TNFα	tumor necrosis factor alpha
TUNEL	terminal deoxynucleotidyl transferase-mediated dUTP nick-end labeling

CHAPTER ONE

LITERATURE REVIEW

I. RICIN

Ricin is a plant toxin that inhibits protein synthesis and is lethal to humans. It is classified by the Centers for Disease Control and Prevention as a Category B (second highest priority) agent due to its high cytotoxicity, abundant availability, and relative ease of production. Ricin is also listed by the Chemical Weapons Convention as a Schedule 1 controlled substance because of its potential for warfare purposes. Ricin can be weaponized into a bioterrorism agent or used as a biochemical agent to contaminate food and water (1). It is speculated that Bulgarian dissident Georgi Markov was assassinated with an umbrella that pierced his leg with a pellet containing ricin.

Ricin is purified from the seeds of the castor bean plant, *Ricinus communis*, which belongs to the family of Euphorbiacear. All parts of the plant are poisonous, but the highest concentration of ricin is present in the seeds. The castor bean plant originated from tropical and subtropical Africa but has spread to all climatic regions of the United States, Asia, and Europe. The castor bean plant has a long history of being grown as an

ornamental plant and for its castor oil. Castor oil is used as a lubricant for engines, a base for paints, raw material for pharmaceutical products, an additive for the food industry, and is orally administrated as a folk remedy to induce bowel movement. Castor oil is currently regulated by the US Food and Drug Administration as an over-the-counter laxative medicine (2). Being a by-product of castor oil production, as much as 35,500 tons of ricin is theoretically produced per year before the detoxification process (3). Several methods for ricin purification have been published in the literature and on the internet, and can easily be obtained by the general public.

Structure and Availability of Ricin

Ricin is a type II ribosome-inactivating protein (RIP) consisting of two polypeptide chains, an RNA *N*-glycosidase A-chain (RTA) and a galactose- or *N*-acetylgalactosamine-specific lectin B-chain (RTB) (Fig. 1) (4). Heterodimeric ricin has a molecular mass of 65 kDa, and its two chains are linked by a disulfide bond. The X-ray structure of ricin has been solved, and crucial sites for substrate binding of ricin have been identified by using site direct mutagenesis of residues (5). The molecular mass of glycosylated RTA is approximately 32 kDa and RTB is 34 kDa. The active site sequence in RTA is highly conserved across all RIPs. Ricin isolated from seeds of five horticultural

varieties of *Ricinus communis* was found by electrospray mass spectrometry to consist of a series of glycosylated proteins, suggesting a large extent of heterogeneity for each cultivar (6).

Transport by Retrograde Translocation

Ricin B-chain facilitates entry of ricin holoenzyme into the cell by binding to carbohydrates of glycoprotein and glycolipid on the cell membrane (Fig. 1). Ricin is internalized by clathrin-coated endocytosis; however, clathrin-independent endocytosis, such as caveolae and macropinocytosis, has also been reported. After ricin enters the cell, the majority of ricin is transported to early endosomes to be recycled to the membrane or to late endosomes and lysosomes to be degraded (7). Using a sulfation assay, ricin was shown to be transported from both early and late endosomes to the trans-Golgi network where tyrosine sulfation of RTA occurs. Ricin is then translocated from the Golgi apparatus to the endoplasmic reticulum (ER) and is glycosylated in the ER by oligosaccharyl transferase. The KDEL sequence present on the C-terminus is required for some RIPs to utilize retrograde translocation from the Golgi complex to the ER. However, ricin does not contain the KDEL sequence, and the specific mechanism that translocates ricin through the ER is unknown (8). RTA and RTB are separated in the ER

by disulphide isomerase, and RTA is translocated to the cytosol, where its ribosome substrates are located (7, 9).

General Toxicity

Although ricin may be inactivated by heat, it is highly cytotoxic and lethal if ingested, inhaled, or injected. The action of ricin poisoning varies depending on the routes of exposure. The LD_{50} of ricin in mice is 22 mg/kg by ingestion; however, it is estimated to be much lower at 3 to 5 μg/kg by intravenous injection or aerosol inhalation (10). Monkeys and rodents exposed to 20 to 40 μg/kg ricin by aerosol inhalation developed necrotizing airway lesions, interstitial edema, and pulmonary inflammation. RTA is also responsible for inducing vascular leak syndrome in humans. A man who committed suicide by intravenous and subcutaneous injection of ricin presented nausea, vomiting, diarrhea, dyspnoea, vertigo and muscular pain. He died due to multi-organ failure in spite of symptomatic and supportive intensive care for 9 hours in the hospital (11). In another suicide case report, injection of ricin caused fever, nausea, vomiting, dehydration, hypotension, hypoglycemia, gastroenteritis, circulatory collapse, multi-organ failure, and death (12).

Treatment

Currently effective antidotes and vaccines for ricin intoxication are under development. A recombinant ricin vaccine, RiVax, has two point mutations of Y80A (the ribotoxic stress-inducing site) and V76M (the vascular leak syndrome-inducing site), and is currently in clinical trials for safety evaluation (13). RiVax is formulated as a lyophilized form to improve its stability and efficacy (14). Administration of RiVax intramuscularly or intradermally protects mice from systemic and mucosal exposure of ricin (15). Recently a retrograde translocation blocker was identified to protect mice from lethal nasal exposure to ricin (16). A cell-based high-throughput screen was also used to identify small molecule inhibitors against ricin (17). Some inhibitors are effective against ricin by binding to the active sites of RTA (18).

Mechanisms of Cytotoxicity

A. Ribosomal RNA depurination

Most of the RTA that enters the cell is degraded by proteasomes in the cytosol but a portion of RTA can escape degradation and reaches the ribosome. RTA irreversibly removes a conserved adenine nucleotide from the sarcin-ricin loop within the eukaryotic 28S ribosomal RNA of the 60S ribosome subunit (19). RTA depurination has a very

strong salt sensitivity and achieves an unusually high k_{cat}/K_m of 10^9-10^{10} $M^{-1}s^{-1,}$ indicating multiple electrostatic interactions with the ribosome (20). A single molecule of RTA depurinates about 1500 mammalian ribosomes per minute in the cytosol, which leads to protein synthesis inhibition (21).

B. Protein synthesis inhibition

Protein synthesis is inhibited by RTA at the translocation step of the elongation cycle. Ribosome depurination blocks the GTP-dependent binding of elongation factor 2 (EF 2) or ADP-ribosyl-EF2 to the ribosome, however, the binding of aminoacyl-tRNA to the ribosome was not affected by ribosome depurination (22, 23). It has generally been assumed that ricin toxicity is due to this inhibition of protein synthesis, as evidenced by the finding that ricin-induced apoptosis is prevented by cycloheximide, a protein synthesis inhibitor. However 3-methyladenine, a specific inhibitor of autophagy also inhibited ricin-induced cell death (24). It has been reported in yeast that nontoxic RTA mutants still depurinate ribosomes and inhibit protein synthesis at a level similar to wild-type RTA, suggesting that ribosome depurination is not sufficient for RTA-induced cytotoxicity in all cases, at least in yeast (25).

C. Ribotoxic stress response

The ribotoxic stress response is characterized by activation of mitogen-activated protein kinase (MAPK) pathways in response to ribosome depurination. The MAPK family comprises the stress-activated protein kinases (SAPK; also known as c-jun N-terminal kinases, or JNK, and the p38 MAP kinase signaling pathway), and the extracellular signal-regulated kinase, ERK. Ultraviolet-B radiation and oxidative stressors such as sodium arsenite or cadmium chloride also trigger the activation of JNK1 through different mechanisms (26). It has been shown that ricin induces the ribotoxic stress response; however, the exact mechanisms have not been determined. It has been speculated that the MAPK signaling pathway may trigger the apoptotic response (27). Cross-talk between the intrinsic apoptotic pathway and the p38 MAPK pathway occurs in the murine macrophage cell line RAW264.7 treated with ricin (28). Ricin induces interleukin 8 secretion by activating p38 MAPK in the human monocyte/macrophage cell line, 28SC (29). Ricin activates all three MAP kinase superfamily members including p38 MAPK, JNK, and ERK in the macrophage cell line RAW264.7 (30). However, the role of the SAPK pathways in ricin-induced apoptosis is not well-described.

D. Apoptosis

Studies from the 1980s showed that ricin lyses cells and induces DNA fragmentation in a process similar to apoptosis (31). Recently, it was shown that ricin

induces mRNA levels of pro-inflammatory cytokines such as TNF-α in primary alveolar macrophages and bone marrow-derived macrophages. The secretion of TNF-α results in engagement of an apoptotic cascade that includes activation of both apical (caspase-8 and caspase-9) and effector (caspase-3) caspases (32). Caspases mediate apoptosis by cleaving aspartic acid residues and activating downstream effectors and substrates. Cleaved (activated) caspase-3 cleaves poly (ADP-ribose) polymerase (PARP) which is responsible for DNA repair. The 116 kDa PARP is cleaved into 89 and 24 kDa inactive fragments, which makes PARP unable to repair DNA. PARP is a widely used marker of apoptosis, and studies have shown that ricin induces apoptosis in terms of PARP cleavage in human cervical cancer HeLa cells and myeloid leukemia U937 cells (33, 34). Over-expressing Bcl-2, an anti-apoptotic protein, partially inhibits ricin-induced apoptosis in the hepatoma cell line BEL7404 (35).

RTA/Immunotoxins

RIPs have been conjugated to antibodies, growth factors, hormones, and lectins to target a selected cell type as anticancer agents (36). RTA can be conjugated to an antibody to form an immunotoxin that is a potential candidate for cancer chemotherapy (37). This hybrid molecule is cytotoxic to the target tumor cells that express the cell-surface antigen. However, the effects of immunotoxins on target cells have only been

examined by measuring protein synthesis inhibition (38). Problems with this therapeutic approach include findings that RTA-based immunotoxins cause vascular leak syndrome which is characterized by hypoalbuminemia, peripheral edema with resultant weight gain, and pulmonary edema in the most severe cases. RTA alone induces endothelial cell permeability in human umbilical vein-derived endothelial cells, suggesting that the RTA component of the immunotoxin molecule is responsible for vascular leak (39).

II. SHIGA-LIKE TOXIN 2 (Stx2)

Stx2, another type II ribosome-inactivating protein, is a bacterial toxin that is produced by many strains of bacteria. Stx2 is composed of one 30 kDa enzymatic A-chain which possesses *N*-glycosidase ability to inactivate the ribosome, and five 7 kDa B-subunits which form a pentamer (40). The pentameric B-chains bind to the globotriaosylceramide (Gb3) receptor in the glycolipid-enriched membrane domain to facilitate cell uptake (41). Similar to ricin, Stx2 A-chain is transported from the ER to the cytosol to inhibit protein synthesis by cleaving one adenine residue on the 28S ribosomal RNA of the 60S ribosomal subunit (42). This depurination inhibits the binding of amino-acyl-tRNA to the ribosome, leading to protein synthesis inhibition (40). Stx2 not only

inhibits protein synthesis but also induces apoptosis and PARP cleavage in a caspase-mediated manner (43).

The most common Stx2 is produced from enterohemorrahagic *Escherichia coli* and is responsible for a large number of infections and death among children and the elderly. One of its infamous serotypes is O157:H7 associated with hemorrhagic colitis and hemolytic uremic syndrome which has complications including thrombocytopenia, microangiopathic hemolytic anemia and renal failure (44). Contamination of milk, juice, and vegetables with Stx2 has been reported. Stx2-producing *E. coli* also produce Stx2 variants Stx2c, Stx2d1, Stx2d2, Stx2e, Stx2f, and Stx2y (43).

Retrograde transport

After binding to the Gb3 receptor, Stx2 is taken up by the cell through clathrin-mediated endocytosis. The lipid composition of the cell surface and the content of the Gb3 receptor determine if cells are sensitive to Stx2. For example, bovine aortic endothelial cells are less sensitive to Stx2 because they lack the globo-series neutral component of the Gb3 receptor (45). After binding to the Gb3 receptor, Stx2 undergoes retrograde translocation from the early endosomes to the Golgi apparatus. This translocation is dependent on the GTP-binding protein Rab9, and Golgi-associated

protein TGN38. In the Golgi apparatus, the A-chain is proteolytically cleaved by furin, resulting in the generation of A_1 and A_2 chains linked by a disulfide bond. The A chains are then transported from the Golgi apparatus to the ER lumen where A_1 is released because of the reduction of the disulfide bond (46). Trafficking of Stx2 to the Golgi apparatus and the ER are required for Stx2 to induce cytotoxicity. In HeLa cells, Stx induces the formation of tyrosine kinase Syk and clathrin heavy chain complex. When Syk is knocked down by siRNA or expressing a kinase dead mutant of Syk, Golgi transportation of Stx was downregulated (47). Stx activates both JNK and p38 signaling pathways in African green monkey kidney epithelial Vero cells and human myelogenous leukemia cells (48, 49). When the p38 MAPK pathway is inhibited by chemical inhibitors or siRNA, Stx-induces cytotoxicity and translocation to Golgi apparatus is reduced (50). Understanding the mechanisms of retrograde translocation of Stx2 is crucial for the development of safe and effective treatment to this public health threat (16).

Treatment

Currently, no effective and safe therapies for preventing or curing Stx2-induced illness are available (51). Knowledge of the Stx2 structure and function will allow us to develop preventive measures or to identify therapeutic targets for Stx2-induced toxicity.

III. OBJECTIVES OF THE THESIS

In summary, ribosome-inactivating proteins (RIPs) are toxins produced from various families of plants, fungi, algae, and bacteria. RIPs are cytotoxic to mammalian cells, and currently effective antidotes and vaccines for their intoxication are under development. RIPs inhibit protein synthesis by cleaving an adenine on the sarcin/ricin loop within the 28S ribosomal RNA of the 60S ribosome subunit. Protein synthesis inhibition has generally been assumed to be responsible for ricin-induced cytotoxicity. However, nontoxic RTA mutants can still inhibit protein synthesis at a level similar to wild-type RTA in yeast. Our ultimate goal is to investigate the relationship between protein synthesis and cytotoxicity using recombinant mutant RTA in the mammalian system. Therefore, the objectives of this work were to: (1) to establish a mammalian cell culture model that is sensitive to exogenous RTA and (2) to investigate the role of SAPK signaling pathways in RTA-induced cytotoxicity. An additional goal was to determine if the ribosomal protein L3delta could inhibit the cytotoxicity of stx 1 and stx 2 in mammalian cells.

CHAPTER TWO

ROLE OF STRESS-ACTIVATED PROTEIN KINASE CASCADES IN RTA-INDUCED CYTOTOXICITY

Introduction

Ricin is a type II ribosome-inactivating protein (RIP) present in seeds of the castor plant, *Ricinus communis* (52). The Centers for Disease Control and Prevention classify ricin as a Category B agent, its second highest priority, because it is extremely toxic and moderately easy to produce and disseminate widely as a bioterrorism agent (1). Ricin is composed of ricin-A-chain (RTA) and ricin-B-chain (RTB) which are linked by a disulfide bond (53). RTB is a lectin that binds to galactose- or N-acetylgalactosamine-containing glycolipids and glycoproteins on the cell surface. It facilitates cell entry of ricin through endocytosis. Approximately 5% of ricin that is endocytosed is transported by retrograde translocation to the trans Golgi network, through the Golgi apparatus, and to the endoplasmic reticulum (ER) (7). After the reduction of the disulfide bond in the ER, RTA reaches the cytosol and avoids proteasomal degradation because of its low lysine content (54). RTA is an *N*-glycosidase that inactivates the ribosome by removing an adenine from the sarcin/ricin loop of the 28S ribosomal RNA (55). This ribosome

depurination prevents the binding of elongation factors to the ribosome and subsequently inhibits protein synthesis (22).

Inhibition of protein synthesis has long been thought to be responsible for the cytotoxicity of ricin as well as other type II RIPs; however, recent evidence suggests that these proteins may activate cell death through other mechanisms (25, 56, 57). Ricin activates the mitogen-activated protein kinase (MAPK) signaling pathways which characterize the ribotoxic stress response (27). Some reports have speculated that the MAPK signaling pathway may trigger apoptosis; however the relationships between ricin-induced MAPK activation and apoptosis have not been well investigated. The objectives of the present study were to investigate if exogenous RTA alone can induce ribotoxic stress and apoptosis, and to determine if specific MAPK signaling pathways are essential for the apoptotic action of RTA.

Materials and methods

Reagents: Dulbecco's Modified Eagle's Medium-high glucose (DMEM-H) and RPMI medium 1640 were purchased from Invitrogen (Carlsbad, CA). Fetal bovine serum (FBS) was purchased from Gemini Bio-Products (West Sacramento, CA). D-Glucose, insulin solution from bovine pancreas, penicillin, streptomycin, gentamicin, phenol red (PR)-free

DMEM and RTA were purchased from Sigma-Aldrich (St. Louis, MO). Ricin, RTA, and RTB were purchased from Vector Laboratories (Burlingame, CA). Sodium bicarbonate, JNK inhibitors SP600125, and p38 inhibitor SB239063 were purchased from EMD Chemicals (Gibbstown, NJ). Falcon tissue culture plasticware (Becton, Dickinson and Company, Franklin Lakes, NJ) was used unless otherwise indicated.

Cell culture: The bovine mammary epithelial cell (MEC) line MAC-T was established from primary bovine mammary alveolar cells immortalized by stable transfection of the Simian virus 40 large T antigen. When MAC-T cells were injected into immunodeficient mice, the mice did not grow tumors after 8 weeks, suggesting that MAC-T cells are not transformed. In addition, when supplied with appropriate substratum and hormones they can be induced to differentiate similar to primary MEC (58). Stock cultures of MAC-T cells were routinely maintained in DMEM-H supplemented with 3.7 g/L sodium bicarbonate, 5 μg/ml insulin from bovine pancreas, 10% FBS, 20 U/ml penicillin, 20 μg/ml streptomycin, and 50 μg/ml gentamicin. HeLa and Vero cells were kind gifts of Dr. Tom Obrig, University of Virginia, Charlottesville, VA. Stock cultures of HeLa cells and Vero cells were routinely maintained in RPMI medium 1640 supplemented with 10% heat inactivated (56°C, 30 minutes) FBS or FBS, respectively, and antibiotics. All cells

were passaged by trypsinization and maintained in a 37°C incubator with 5% CO_2.

Caspase 3/7 Assay: Caspase 3/7 activation was measured using the SensoLyte Homogeneous AMC Caspase 3/7 Assay kit according to the manufacturer's protocol (AnaSpec, Fremont, CA). This assay kit detects the fluorescence intensity of the amino acid aspartic acid-glutamic acid-valine-aspartic acid-AMC which is the substrate of both caspase 3 and 7. Cells were grown in 96-well flat clear bottom black polystyrene cell culture-treated microplates (Corning, Corning, NY). Cells were grown in defined media described above for stock cultures, with the exception that MAC-T cells were plated in PR-free media. Cells were grown to confluence, washed twice with phosphate buffered saline (PBS), and incubated in PR-free DMEM-H (MAC-T cells) or RPMI medium 1640 supplemented with antibiotics, 0.2% bovine serum albumin (BSA), and 30 nM sodium selenite during the serum-free washout period. The spent media were aspirated and replaced with serum-free media without additives and supplemented with antibiotics ± treatments for various times. Caspase-3/7 substrate solution was added to each well to lyse the cells without removing the media, and the microplate was incubated at room temperature for one hour on an orbital incubator at 150 rpm. The microplate was kept away from direct light and fluorescence intensity was measured at

excitation/emission=360 nm/460 nm using a Synergy HT Multi-Mode Microplate Reader (BioTek Instruments, Winooski, VT).

Ribosomal RNA depurination assay: Ribosomal RNA (rRNA) depurination was analyzed by dual-primer extension as described previously (59). MAC-T cells were grown to confluence in 60 mm cell culture dishes (Becton, Dickinson and Company), serum-starved, and treated as described above for caspase assays. After treatment, MAC-T cells were lysed in Trizol (Invitrogen), and total RNA was extracted using RNeasy columns (Qiagen, Valencia, CA). RNA concentration was determined by using a Thermo Scientific Nano Drop 1000 Spectrophotometer (Thermo-Fisher Scientific, Waltham MA). RNA integrity was assessed by running RNA samples on an agarose gel stained with ethidium bromide and checking 18S and 28S rRNA. Total RNA (2 μg) isolated from MAC-T cells was hybridized with 10^6 cpm of two primers end-labeled with [γ-^{32}P]ATP (Perkin-Elmer, Waltham, MA) using T4 kinase (Invitrogen). The depurination primer (5′-AACAGATGGTAGTTTCACCCC-3′) annealed 64 nucleotides (nt) 3′ of the depurination site on the 28S rRNA and the 28S control primer (5′-TTCACTCACCGTTACTGAGG-3′) annealed 99 nt 3′ of the 5′ end on the 28S rRNA. rRNA depurination was verified by the synthesis of 64 nt product which was terminated at the depurination site. The end-labeled

28S primer was diluted 1:4 with unlabeled 28S primer to conduct accurate quantification, and the 99 nt products were used as an internal control. SuperScript II Reverse Transcriptase (Invitrogen) was then used in the dual primer extension assay. Extension products for the depurination and control fragments (64 nt and 99 nt, respectively) were separated on a 7 M urea-5% polyacrylamide denaturing gel. The extent of rRNA depurination was analyzed by scanning and quantifying the bands using a Storm PhosphorImager (GE Healthcare, Piscataway, NJ).

Protein Synthesis Assay: Confluent MAC-T cells were serum-starved, washed two times with PBS, and incubated with methionine-free DMEM-H for 45 min prior to treatment. Cells were incubated with 15 μCi [^{35}S]methionine (MP Biomedicals, Solon, OH) during the last hour of treatment. Cells were washed two times with PBS and scraped into 5% trichloroacetic acid (TCA). Samples were centrifuged for 15 min at 3600 rpm. Pellets were washed three times with ice-cold 5% TCA and resuspended in 0.1 M NaOH. Radioactivity was determined by scintillation counting (Beckman Coulter, Brea, CA).

***Small interfering (si) RNA transfection*:** MAC-T cells were plated at 3×10^4 cells/cm^2 in PR-free DMEM-H. The next day, cells were transfected in DMEM-H supplemented with antibiotics with 88-172 nM siRNA (Thermo-Fisher Scientific) using GeneEraser (Agilent

Technologies, Santa Clara, CA) according to the manufacturer's protocol. After 2.5 days, cells were washed with serum-free media for 2 h, and incubated in PR-free DMEM-H supplemented with antibiotics ± treatments. After 6 h, cell lysates were collected and analyzed by Western immunoblotting or caspase-3/7 assay.

Western immunoblotting: MAC-T cells were grown to confluence in 60 mm cell culture dishes, serum-starved, and treated with RTA. After treatment, cell culture dishes were placed on ice, and cells were washed with cold PBS. Cell lysates were collected in lysis buffer (1% Triton X-100, 50 mM Hepes buffer without sodium, 80 mM B-glycerophosphate, 2 mM ethylenediaminetetraacetic acid, 2 mM ethylene glycol tetraacetic acid, 10 mM sodium fluoride, 0.1% sodium dodecyl sulfate (SDS), 2 mM sodium orthovanadate, 2 mM phenylmethylsulfonyl fluoride, 10 μg/ml leupeptin, 10 μg/ml aprotinin, and 10 μg/ml trypsin inhibitor), incubated on ice for 30 min, and centrifuged at 13000 g for 15 min at 4°C. Protein concentration was determined using a Bradford protein assay (Bio-Rad Laboratories, Hercules, CA) using BSA as a standard. Proteins were reduced and denatured by β-mercaptoethanol and SDS, respectively. Equal amounts of protein were separated by SDS-polyacrylamide gel electrophoresis (PAGE) under reducing conditions. SDS-PAGE gels were wet-transferred to Trans-Blot transfer

medium nitrocellulose membrane (0.2µm; Bio-Rad Laboratories), Immun-Blot polyvinylidene fluoride (PVDF) membrane (0.45µm; Millipore, Billerica, MA), or Immobilon-P transfer (PVDF) membrane (0.2µm; Bio-Rad Laboratories). Membranes were blocked in tris buffered saline (TBS) + 0.5% tween (TBS-T) with 5% non-fat dried milk for one hour at room temperature, and then incubated with primary antibody overnight at 4°C. Antibodies against poly(ADP-ribose) polymerase (PARP), JNK, p38, phospho-p38, cleaved caspase 3, cleaved caspase 7, and phospho-c-jun (Cell Signaling Technology, Danvers, MA), phospho-JNK (Santa Cruz Biotechnology), actin (EMD Chemicals) and HSP60 (Abcam, Cambridge, MA) were used to detect the corresponding proteins. Membranes were washed with TBS-T, and then incubated with horseradish peroxidase-conjugated secondary antibodies (anti-rabbit IgG and anti-mouse IgG; GE Healthcare and Vector Laboratories, respectively). Membranes were again washed with TBS-T, and incubated with Pierce enhanced chemiluminescence Western blotting substrate (Thermo-Fisher Scientific) to detect peroxidase activity. Membranes then were stripped with Restore plus Western Blot stripping buffer (Thermo-Fisher Scientific) and reprobed with antibodies for total protein as loading controls. X-ray film development was used for luminescence measurement.

Terminal deoxynucleotidyl transferase-mediated dUTP nick-end labeling (TUNEL) staining: MAC-T cells were plated at a concentration of 1×10^4 cells/cm^2 on glass chamber slides (Becton, Dickinson and Company). Confluent cells were serum-starved for 16 h and then treated with RTA. After toxin treatment, cells were fixed with 4% paraformaldehyde and permeabilized using 0.1% sodium citrate and 0.1% Triton X-100. Cells were stained using the In Situ Cell Death Detection kit (Roche Diagnostics Corporation, Indianapolis, IN) according to the manufacturer's protocol. This kit measures apoptosis by labeling fragmented DNA using tetramethylrhodamine-dUTP. After counterstaining with Hoechst 33342 (Invitrogen), slides were examined under a Nikon Eclipse E800 fluorescent microscope. Images were captured with ACT-1 software.

Statistical analysis: Data were analyzed by one-way ANOVA with Dunnett's Multiple Comparison post-test or two-way ANOVA (with repeated measures where appropriate) with Bonferroni post-tests using GraphPad Prism Software.

Results

MAC-T cells are more sensitive to RTA than Vero or HeLa cells

It has previously been shown in our laboratory that a protein synthesis inhibitor, anisomycin, induces apoptosis of MAC-T cells; therefore, we examined if RTA would

induce apoptosis in MAC-T cells, since both proteins act on the ribosome. Other mammalian epithelial cell lines, HeLa and Vero cells, were used to compare their responsiveness to RTA. Since ricin can be used as a bioterror weapon that could potentially be delivered by aerosolization to humans, mammalian epithelial cells have been used to study its cytotoxicity. Caspase 3 and 7 are essential to the execution phase of apoptosis, and their activities are commonly used as indicators of apoptosis. As shown in Fig. 2A and 2B, 1 μg/ml RTA induced caspase-3/7 activity in a time-dependent manner in MAC-T cells, suggesting that MAC-T cells are responsive to RTA. RTA induced significantly higher caspase-3/7 activity in MAC-T cells compared to Vero cells. RTA induced caspase-3/7 activity 12-fold over untreated controls at 4 h ($P < 0.01$) and the increase was maintained at 14-fold through 6 h ($P < 0.01$) in MAC-T cells (Fig. 2A). While RTA induced a 7-fold increase in caspase-3/7 activity at 6 h in HeLa cells, significantly higher caspase-3/7 activity was induced in MAC-T cells relative to HeLa cells at both 4 and 6 h ($p < 0.001$, $p < 0.05$, respectively, Fig. 2B). Therefore, we used MAC-T cells in this study since they are the most sensitive cell line compared to Vero and HeLa cells.

RTA and ricin induce similar maximal increases in caspase-3/7 activity in MAC-T cells but ricin is more effective at lower concentrations

Once we identified that MAC-T cells represented a sensitive cell line to study ricin action, MAC-T cells were treated with increasing concentrations of RTA alone or ricin holoenzyme for 4 h. A delayed concentration-dependent increase in caspase-3/7 activity was observed when MAC-T cells were treated with RTA compared to ricin. Ricin induced significantly higher caspase-3/7 activity at low concentrations (0.0001 – 0.01 μg/ml) compared to RTA ($p < 0.05$, Fig. 3); however, no differences in caspase-3/7 activity were observed between ricin and RTA at higher concentrations (0.1 to 10 μg/ml). These data suggest that RTA enters the cell with a lower efficiency relative to ricin in the absence of RTB, but ultimately is able to induce a similar degree of caspase-3/7 activation at higher concentrations.

RTA from Vector Laboratories induces caspase-3/7 activity less efficiently than RTA isolated from Sigma while RTB has no effect

To determine if MAC-T cells responded similarly to RTA obtained from different suppliers, MAC-T cells were treated with RTA from Sigma and Vector Laboratories. Both sources of RTA induced caspase-3/7 activity in MAC-T cells; however, the increase

in caspase activation after 4 h of treatment was significantly greater in cells treated with RTA from Sigma relative to Vector Laboratories (Fig. 4A). To determine if this difference was related to a difference in the dose-response curve, MAC-T cells were treated with increasing concentrations of RTA for 6 h. There was no significant difference between the two forms of RTA in terms of caspase-3/7 activity at relatively high concentrations (1 and 10 μg/ml); however, RTA obtained from Sigma had significantly higher caspase-3/7 activity relative to RTA obtained from Vector Laboratories at 0.01 to 0.1 μg/ml of RTA ($P < 0.001$, Fig. 4B). Additionally, 10 μg/ml RTB was unable to induce caspase-3/7 activity in MAC-T cells over a 6-h treatment. These data suggest that RTA obtained from Sigma induces apoptosis more efficiently than the RTA obtained from Vector Laboratories and that RTB alone has no biological effect in the cell.

RTA from Sigma is not contaminated with RTB

One possibility for the enhanced responsiveness of cells to Sigma RTA at lower concentrations was that it contained some RTB, which could facilitate cell entry. As shown in Fig. 5, western immunoblot analysis showed that neither RTA from Sigma nor RTA from Vector Laboratories contained RTB (Fig. 5A). Conversely, no RTA was

observed in RTB (Fig. 5B). Two bands of glycosylated RTA were observed, and were seen at approximately 29 and 32 kDa.

One hour of exposure to RTA induces similar caspase-3/7 activity compared to exposure over the entire treatment interval

For this experiment, MAC-T cells were treated with RTA for the entire treatment interval, as in previous experiments, or RTA was removed after 1 h, cells were rinsed, and media were replaced with serum-free media for the remaining time. Interestingly, there were no differences in caspase-3/7 activity between cells exposed to RTA for 1 h compared to the entire treatment interval (Fig. 6).

RTA depurinates the α-sarcin/ricin loop of 28S rRNA and inhibits protein synthesis

To further examine cytotoxicity of RTA in MAC-T cells, we analyzed ribosome depurination and protein synthesis. Total RNA was isolated from MAC-T cells, and depurination of rRNA was examined by dual-primer extension assay. A depurination primer was used to measure the extent of rRNA depurination, and the 28S rRNA primer was used to measure the total amount of 28S rRNA in the primer extension reaction. The extent of ribosome depurination was quantified by densitometry and normalized by the

total amount of 28S rRNA. Ribosome depurination was observed in the MAC-T cells which were treated with either 0.1 or 1 μg/ml RTA. The highest level of ribosome depurination was observed with 1 μg/ml RTA after 6 h of treatment (Fig. 7A). Although ribosome depurination was relatively similar at 6 h for both concentrations tested, there were differences between the two concentrations at 2 and 4 h (5% vs. 42%, 51% vs. 89%, respectively, Fig. 7B). Inhibition of protein synthesis is associated with ribosome depurination. Therefore, the protein synthesis status was investigated by [^{35}S]-methionine incorporation. Results were similar to ribosome depurination; 1 μg/ml RTA inhibited protein synthesis approximately 50% by 2 h, with maximal inhibition observed at 4.5 h. RTA maximally inhibited protein synthesis at 4.5 h for both concentrations tested, but there were significant differences between the two concentrations at 2 h (91% vs. 50%) and at 3 hours (77% vs. 4%, Fig. 8).

Caspase-3/7 cleavage, PARP cleavage and TUNEL staining indicate that RTA effectively induces apoptosis

To gain further insight into the ability of RTA to induce apoptosis in MAC-T cells, we investigated a broader spectrum of molecular assays. Since the SensoLyte Homogeneous AMC Caspase-3/7 Assay kit detects a shared fluorogenic substrate, Ac Asp-Glu-Val-

Asp-AMC, from both caspase 3 and caspase 7, this assay cannot distinguish between activation of these two caspases. In order to determine which caspase was activated by RTA in MAC-T cells, we performed Western immunoblotting using specific antibodies for their cleaved forms. RTA induced caspase 3 and 7 cleavage in a time- and concentration-dependent manner with RTA treatment (Fig. 9A). Caspase 3 has been reported to cleave PARP which is involved in DNA repair and is used as a marker of late-stage apoptosis. Similar to the caspase 3 and 7 cleavage data, 1 μg/ml RTA induced PARP cleavage at 4 h. In addition, an interesting observation was the similar PARP cleavage observed when cells were exposed to RTA for only 1 h compared with the entire treatment interval (Fig. 9B). As shown in Fig. 10, TUNEL staining was also observed. Disintegrated nuclei were observed after 4 h exposure of 1 μg/ml RTA.

The JNK signaling pathway plays a major role in RTA-induced apoptosis

Since ricin activated both the JNK and p38 signaling pathways, we were interested in determining which of these pathways were involved in RTA-induced apoptosis. Ricin activated JNK1, JNK2 and p38 within 1 h of treatment compared to RTA alone. While RTA alone had no effect at this time point, RTA did activate these signaling molecules at 2 h (Fig. 11A). Both JNK and p38 MAPK pathways maintained their activation through

8 h of treatment with either holoenzyme or RTA (Fig. 11B). To examine the roles of specific signaling pathways in apoptosis, specific signaling molecules were inhibited using chemical inhibitors. Using the JNK pathway inhibitor SP600125, c-jun phosphorylation was reduced by approximately 50%; however, a total knockdown in p38 phosphorylation was observed with the p38 inhibitor SB239063 (Fig. 12). When the JNK signaling pathway was inhibited by SP600125, RTA induced significantly lower caspase-3/7 activity compared with that observed with an intact JNK signaling pathway. However, in the presence of the p38 signaling pathway inhibitor, SB239063, RTA induced similar levels of caspase-3/7 activity (Fig. 13A). A similar pattern was observed with RTA-induced caspase 3 cleavage via Western immunoblotting; JNK inhibition decreased the ability of RTA to induce caspase 3 activation but not p38 inhibition (Fig. 13B). In contrast, inhibition of either the JNK or p38 signaling pathway had a significant influence on RTA-induced PARP cleavage.

Transfection with small interfering (si) RNA was used to verify the results of the inhibitor studies. Transfection of siRNA specific to JNK2 or p38α knocked down both phosphorylated and total protein expression of JNK or p38 respectively (Fig. 14A). In the presence of JNK2 siRNA, either 0.1 or 1 μg/ml RTA induced significantly less caspase-3/7 activity compared to p38α siRNA (Fig. 14B). Similar results were observed with

PARP cleavage; inhibition of the JNK signaling pathway reduced the ability of RTA to induce PARP cleavage (Fig. 14C). Collectively, our data suggest that the JNK signaling pathway plays a more important role than p38 pathway in mediating RTA-induced apoptosis.

Discussion

The major goal of this study was to investigate the effects of exogenous RTA on apoptosis in a non-transformed epithelial cell line and to determine the role of mitogen activated protein kinase pathways in this response. The analyses of 28S rRNA depurination and protein synthesis inhibition showed that RTA alone could enter MAC-T cells and arrive at the ribosome fairly rapidly to elicit these effects. Additionally, we observed that the MAPK pathways p38 and JNK were activated, indicating that ribotoxic stress was induced. Ribotoxic stress is defined as the activation of MAPK pathways in response to ribosomal damage. It is also induced by agents such as short-wavelength UV light, the tumor promoters arsenite and palytoxin, hyperosmotic shock, proinflammatory cytokines, or withdrawal of a trophic factor (27). In order to determine which of these pathways were more important in apoptosis in response to RTA, chemical inhibitors and siRNAs were used to inhibit activation of each pathway. We demonstrated that the JNK

pathway plays a more important role than the p38 MAPK pathway in RTA-induced apoptosis.

The nontransformed mammalian epithelial cell line MAC-T has served as a useful cell culture system in our laboratory for ribotoxic stress and apoptotic studies (60); therefore, we hypothesized that the MAC-T cell line would be a suitable cell culture system for studying RIP-induced cytotoxicity. We first measured activation of the executioner caspases 3 and 7 in RTA-treated MAC-T, HeLa, and Vero cells. Surprisingly, we observed apoptotic activation in MAC-T cells with the treatment of RTA in the absence of RTB within 2 to 4 h. Our data showed that MAC-T cells were more sensitive to RTA than HeLa or Vero cells. It has been reported that in human umbilical vein-derived endothelial cells, human embryonic kidney 293 and HeLa cells, RTA alone induces very low levels of cytotoxicity (39, 61). Although we showed that RTA activated very little apoptosis in Vero cells, we observed that another RIP, Shiga-like toxin 2 (Stx2) did activate apoptosis as well as depurination in these cells (see Chapter three). The cell type specificity of RIP surface receptors may explain the observed differences in susceptibility to different RIPs, as the pentamer of Stx2-B-chain binds to the globotriaosylceramide (Gb3) receptor on the cell membrane (62). MAC-T

cells may contain a surface protein that is not present on Vero cells that allows the RTA chain to bind and enter the cells in the absence of RTB.

RTB facilitates entry of ricin holoenzyme into cells by binding to the glycolipid or glycoprotein on the cell membrane, and RTA contains the enzymatic activity that irreversibly inactivates the ribosome (7). Although it is generally accepted that RTB is required for ricin holoenzyme to induce cytotoxicity, a few research groups have reported the comparison between RTA and ricin holoenzyme in other cell lines. In HeLa cells, 33.4 nM of recombinant RTA was needed to inhibit protein synthesis 50% compared to 3.3 pM of ricin holoenzyme within 6 h (63). In Vero cells, 200 ng/ml of recombinant RTA inhibited 50% of protein synthesis compared to 1 to 2 ng/ml of ricin holoenzyme (64). In the human T-leukemia cell line CEM, an immunotoxin consisting of RTA needed more time to inhibit protein synthesis by one order of magnitude compared to ricin holoenzyme (60 h vs. 2 h) (38). Accordingly, these data indicate that RTA alone inhibits protein synthesis relatively ineffectively in many cell lines compared to ricin holoenzyme. It was proposed that RTA may enter these cells by fluid phase mechanisms in the absence of RTB-binding to the cell membrane (65). When HEK293 and HeLa cells were treated with RTA and RTB-expressing recombinant adenovirus together, a higher degree of cell death was observed relative to that treated with RTA alone (61). These data

agree with the present work, which showed that RTA and ricin holoenzyme exhibited different dose-response curves in terms of their ability to activate caspase-3/7 in MAC-T cells. We showed that a high concentration of RTA alone induced apoptosis relative to a low concentration of ricin holoenzyme (0.0001 – 0.01 μg/ml), which represented an approximate 1000-fold difference. It was also reported that fluid phase uptake of RTA and pokeweed antiviral protein (PAP) are similar and essentially homogeneous (65). PAP is a single chain RIP and thus has no specialized mechanism to enter cell membranes. The mannose receptors on the cell membrane of macrophages were identified to be involved in entry of ricin (66). However, while the present study highlights the validation of a suitable cell culture system for analyzing RTA-induced cytotoxicity, we have not determined if MAC-T cells possess mannose receptors. This study utilized multiple methods for quantitating apoptosis, including caspase-3/7 activation, PARP cleavage, and TUNEL assay. Overall, the results provided convincing evidence that RTA induces cytotoxicity in the absence of RTB, which may have implications for developing therapies against ricin intoxication.

The cytotoxicity of RTA has been characterized by inhibition of protein synthesis, inhibition of cell proliferation, or trypan blue staining (9). Few studies have actually investigated the effects of ricin or RTA on apoptosis in relation to signaling mechanisms.

Overall, we found that the JNK pathway played a greater role in RTA-induced caspase activation and apoptosis compared to p38 MAP kinase pathway. In contrast, significantly lower ricin-induced apoptosis was observed in the presence of a p38 MAP kinase inhibitor in the murine macrophage-like cell line RAW264.7; however, the effects of JNK pathways on ricin-induced apoptosis were not examined (28). Several studies have examined the role of SAPK pathways in ricin induction of proinflammatory markers such as TNF-α and interleukin-1/8 (29, 30, 67). Ricin induces activation of p38, JNK, and ERK signaling pathways, as well as TNF-α mRNA levels in a murine monocyte/macrophage cell line (29). When these MAPK pathways are knocked-down with chemical inhibitors, TNF-α mRNA levels are not increased in response to ricin. They also observed p38, JNK, and ERK phosphorylation in the kidney of ricin-treated mice (30). Similarly, a significant decrease in the ricin-induced proinflammatory response was observed in the presence of a p38 MAP kinase inhibitor in human primary airway epithelial cells (68). The p38 MAPK pathway is required for ricin to induce interleukin-8 expression in the human monocyte/macrophage cell line 28SC (29). Collectively, the p38 MAPK pathway plays an important role in proinflammatory gene expression induced by ricin.

Ricin toxicity may arise from intoxication due to multiple administration routes, including ingestion, injection, or inhalation (1). Therefore, it is not surprising that ricin poisoning is characterized by death due to multiorgan failure or cardiovascular collapse. In a rat model system with ricin aerosol inhalation, ricin induced destructive inflammatory damage in the lung (12). When mice were exposed to ricin, epithelial necrotic and apoptotic cells were observed in the intestine (69). Our understanding of the interactions between ribotoxic stress, SAPK pathways, and apoptosis still remains vague due to the complexity of the mechanism. Identifying the molecular components of ricin intoxication in a mammalian cell model will provide information needed to develop effective therapies against ricin poisoning.

In this study, a nontransformed epithelial cell culture system which is sensitive to RTA alone has been established for future mechanistic research. Additionally, these data suggest that the JNK pathway plays an important role in apoptosis which is induced by RTA. Identification of potential links between ribosome depurination and apoptosis are important for success in detailing molecular mechanisms of ricin toxicity in mammalian systems. Future studies using the differences between ribosome depurination and cytotoxicity of mutant RTA selected by mutagenesis may bring insight into the

relationship between ribotoxic stress, SAPK pathways, and apoptosis in mammalian cells.

CHAPTER THREE

EFFECT OF RIBOSOMAL PROTEIN L3 DELTA ON CYTOTOXICITY OF SHIGA-LIKE TOXINS

Introduction

The shiga-like toxin (Stx) family contains Shiga-like toxin 1 (Stx1) and Shiga-like toxin 2 (Stx2) which are produced by bacteria (70). The most common Stx is produced from enterohemorrahagic *Escherichia coli* and is responsible for many incidences of food borne infectious disease and death occurring in the United States. Stx causes diarrhea, hemorrhagic colitis, and hemolytic uremic syndrome (HUS). The young and the elderly are the most susceptible to the HUS for which no effective treatments are available (71). Stx belongs to a family of ribosome-inactivating proteins (RIP) which includes ricin and pokeweed antiviral protein (PAP). Stx is composed of one Stx-A-chain and pentameric Stx-B-chains which are associated non-covalently. Stx-B-chains bind to the globotriaosylceramide receptor on the cell membrane and facilitate cell uptake of the toxin. Stx undergoes retrograde translocation to the Golgi apparatus where the catalytic A-chain is cleaved by furin to generate an active Stx-A_1 and Stx-A_2 fragments (72). Stx-A_1 and Stx-A_2 remain associated by a disulfide bond and are then translocated to the

endoplasmic reticulum (ER). In the ER, the disulfide bond is reduced and Stx A_1 is released to the cytosol. Stx-A-chain possesses *N*-glycosidase activity which cleaves an adenine from the highly conserved sarcin/ricin loop on the 28S ribosomal RNA of the large ribosomal subunit (40). This depurination interferes with the binding of amino acyl-tRNA and the binding of elongation factor 2 to the ribosome, leading to protein synthesis inhibition. Stx also induces apoptosis in a caspase-mediated manner in mammalian cells (73).

Stx2 inhibits protein synthesis in a rabbit reticulocyte lysate but not in *E. coli* lysates or wheat germ, while PAP inhibits protein synthesis equally among all kingdoms (74). It has been suggested that this variation in sensitivity to rRNA may be due to the difference in the interaction between the specific RIP and ribosomal proteins. It has been shown that in yeast PAP binds to ribosomal protein L3, a highly conserved protein located at the peptidyltransferase center, in order to depurinate the ribosome (75). Additionally, a chromosomal mutant of yeast, which expressed mutant L3, prevented PAP from binding to and depurinating the ribosome.

Since PAP and Stx are both ribosome inactivation proteins targeting the same substrate, the ribosome, an N-terminal fragment of yeast ribosomal protein L3 (L3Δ99), corresponding to the first 99 amino acids of L3, was proposed to play a role in Stx-

induced cytotoxicity. It has also been shown in tobacco plants that co-expression of L3Δ99 with PAP prevented PAP-induced ribosome depurination (76). In addition, expression of Stx1 A-chain (Stx1a) or Stx2 A-chain (Stx2a) induced cytotoxicity in yeast (Tumer, unpublished). Stx1a and Stx2a, which are the active *N*-glycosidase subunits of Stx, have molecular weights of 32 kDa and 33 kDa, respectively. The nucleotide sequence of Stx1a and Stx2a shares 57% homology. Despite the low level of homology between them, Stx1 and Stx2 have similar secondary structures (77). Co-expression of L3Δ99 with Stx1a or Stx2a in yeast resulted in an inhibition in the lethality of both toxins (Tumer, unpublished). The objectives of the present study were to examine the role of L3Δ99 in Stx-induced ribosome depurination and apoptosis in mammalian cells.

Materials and methods

Reagents: RPMI medium 1640 was purchased from Invitrogen (Carlsbad, CA). Fetal bovine serum (FBS) was purchased from Gemini Bio-Products (West Sacramento, CA). Penicillin, streptomycin, and gentamicin were purchased from Sigma-Aldrich (St. Louis, MO). Stx2 was purchased from List Biological Laboratories (Campbell, CA). Falcon tissue culture plasticware (Becton, Dickinson and Company, Franklin Lakes, NJ) was used unless otherwise indicated.

Cell culture: HeLa and Vero cells were kind gifts of Dr. Tom Obrig, University of Virginia, Charlottesville, VA. Stock cultures of HeLa cells and Vero cells were routinely maintained in RPMI medium 1640 supplemented with 10% heat inactivated (56°C, 30 minutes) FBS or FBS, respectively, and antibiotics. All cells were passaged by trypsinization and maintained in a 37°C incubator with 5% CO_2.

Caspase 3/7 Assay: Caspase 3/7 activation was measured using the SensoLyte Homogeneous AMC Caspase 3/7 Assay kit according to the manufacturer's protocol (AnaSpec, Fremont, CA). Cells were grown in 96-well flat clear bottom black polystyrene cell culture-treated microplates (Corning, Corning, NY). Cells were grown to confluence, washed twice with phosphate buffered saline (PBS), and incubated in RPMI medium 1640 supplemented with antibiotics, 0.2% bovine serum albumin (BSA), and 30 nM sodium selenite during the serum-free washout period. The spent media were aspirated and replaced with serum-free media without additives and supplemented with antibiotics ± treatments for various times. Caspase-3/7 substrate solution was added to each well without removing the media, and the microplate was incubated at room temperature for one h on an orbital incubator at 150 rpm. The microplate was kept away from direct light and fluorescence intensity was measured at excitation/emission=360

nm/460 nm using a Synergy HT Multi-Mode Microplate Reader (BioTek Instruments, Winooski, VT).

Ribosomal RNA depurination assay: Ribosomal RNA (rRNA) depurination was analyzed by dual-primer extension as described previously (59). Vero cells were grown to confluence in 60 mm cell culture dishes (Becton, Dickinson and Company), serum-starved, and treated as described above for caspase assays. After treatment, cells were lysed in Trizol (Invitrogen), and total RNA was extracted using RNeasy columns (Qiagen, Valencia, CA). RNA concentration was determined by using a Thermo Scientific Nano Drop 1000 Spectrophotometer (Thermo-Fisher Scientific, Waltham MA). RNA integrity was assessed by running RNA samples on an agarose gel stained with ethidium bromide and checking 18S and 28S rRNA. Total RNA (2 μg) isolated from cells was hybridized with 10^6 cpm of two primers end-labeled with [γ-^{32}P]ATP (Perkin-Elmer, Waltham, MA) using T4 kinase (Invitrogen). The depurination primer (5′-CACAGATGGTAGCTTCGCCCC-3′) annealed 73 nucleotides (nt) 3′ of the depurination site on the 28S rRNA and the 28S control primer (5′- TTCACTCGCCGTTACTGAGG-3′) annealed 99 nt 3′ of the 5′ end on the 28S rRNA. rRNA depurination was verified by the synthesis of 73 nt product which was terminated at the depurination site. The end-

labeled 28S primer was diluted 1:4 with unlabeled 28S primer to conduct accurate quantification, and the 99 nt products were used as an internal control. SuperScript II Reverse Transcriptase (Invitrogen) was then used in the dual primer extension assay. Extension products for the depurination and control fragments (73 nt and 99 nt, respectively) were separated on a 7 M urea-5% polyacrylamide denaturing gel. The extent of rRNA depurination was analyzed by scanning and quantifying the bands using a Storm PhosphorImager (GE Healthcare, Piscataway, NJ).

Western immunoblotting: Vero cells were grown to confluence in 60 mm cell culture dishes, serum-starved, and treated with Stx2. After treatment, cell culture dishes were placed on ice, and cells were washed with cold PBS. Cell lysates were collected in lysis buffer as described in chapter two, incubated on ice for 30 min, and centrifuged at 13000 g for 15 min at 4°C. Protein concentration was determined using a Bradford protein assay (Bio-Rad Laboratories, Hercules, CA) using BSA as a standard. Proteins were reduced and denatured by β-mercaptoethanol and SDS, respectively. Equal amounts of protein were separated by SDS-PAGE under reducing conditions. Gels were wet-transferred to Trans-Blot transfer medium nitrocellulose membrane (0.2μm; Bio-Rad Laboratories), Immun-Blot PVDF membrane (0.45μm; Millipore, Billerica, MA), or Immobilon-P

transfer (PVDF) membrane (0.2μm; Bio-Rad Laboratories). Membranes were blocked in tris buffered saline (TBS) + 0.5% tween (TBS-T) with 5% non-fat dried milk for one h at room temperature, and then incubated with primary antibody overnight at 4°C. Antibodies against poly(ADP-ribose) polymerase (PARP), JNK, p38, and phospho-p38 (Cell Signaling Technology, Danvers, MA), phospho-JNK (Santa Cruz Biotechnology, Santa Cruz, CA), , V5 (Invitrogen), and akt (Millipore) were used to detect the corresponding proteins. Membranes were washed with TBS-T, and then incubated with horseradish peroxidase-conjugated secondary antibodies (anti-rabbit IgG and anti-mouse IgG; GE Healthcare and Vector Laboratories, respectively). Membranes were again washed with TBS-T, and incubated with Pierce enhanced chemiluminescence Western blotting substrate (Thermo-Fisher Scientific) to detect peroxidase activity. Membranes then were stripped with Restore plus Western Blot stripping buffer (Thermo-Fisher Scientific) and reprobed with antibodies for total protein as loading controls. X-ray film development was used for luminescence measurement.

***Transfection*:** Vero cells were plated at 4×10^4 cells/cm^2 in RPMI 1640 medium supplemented with 10% FBS and antibiotics in 96-well flat clear bottom black polystyrene microplates. The next day, cells were transfected in RPMI 1640 medium

supplemented with antibiotics with 0.2 μg total plasmid DNA using Turbofect in vitro Transfection Reagent (Fermentas Life Sciences, Glen Burnie, MD) according to the manufacturer's protocol. After 22 hours, caspase 3/7 activity was measured using the SensoLyte Homogeneous AMC Caspase 3/7 Assay kit according to the manufacturer's protocol (AnaSpec, Fremont, CA). For detection of transfected proteins, Vero cells were plated in 6-well polystyrene plates and transfected as described above with 4 μg total DNA. After 22 hours, cells lysates were collected and analyzed by Western immunoblotting.

Statistical analysis: Data were analyzed by one-way ANOVA with Dunnett's Multiple Comparison post-test or two-way ANOVA (with repeated measures where appropriate) with Bonferroni post-tests using GraphPad Prism Software.

Results

Stx2 induces caspase-3/7 activity in Vero and HeLa cells

Vero cells represent a sensitive cell line to study Stx-induced cytotoxicity, although other cell lines also respond to Stx2 with varying sensitivities, including HeLa cells (78-80). Therefore, Vero and HeLa cells were used as cell culture models to study Stx2-induced apoptosis. To determine if exogenous Stx2 induced apoptosis in Vero and HeLa cells, we

measured caspase-3/7 activation. Caspase 3 and 7 are essential to the execution phase of apoptosis, and their activities are commonly used as indicators of apoptosis. As shown in Fig. 15, increasing concentrations of Stx2 induced caspase-3/7 activity in Vero and HeLa cells. 1 μg/ml Stx2 induced significantly higher caspase-3/7 activity in Vero cells compared to HeLa cells (10-fold and 5-fold, respectively, $p < 0.05$); however, differences in caspase-3/7 activation observed between cell types at lower concentrations (0.001 to 0.01 μg/ml) were not significant. These data suggested that Vero cells are more sensitive to Stx2 than HeLa cells at higher concentrations of the toxin.

To determine the time course of caspase activation by Stx2 in Vero cells, Vero cells were treated with 0.1 μg/ml Stx2 and caspase-3/7 activity was measured for the indicated times. Stx2 induced caspase-3/7 activity 5-fold relative to untreated controls at 6 h in Vero cells (Fig. 16A). Greater increases in caspase activation were observed when cells were treated for longer time intervals. Stx2 induced caspase-3/7 activity 31- and 73-fold relative to untreated controls at 12 and 16 h, respectively, as shown in Fig. 16B, while treatment for 24 h increased caspase activation approximately 100-fold. This high-level of Stx2-induced caspase-3/7 activation was maintained through 36 h (Fig. 16C).

Stx2 depurinates the α-sarcin/ricin loop of 28S rRNA

To further examine cytotoxicity of Stx2 in Vero cells, we analyzed ribosome depurination. Total RNA was isolated from Vero cells, and depurination of ribosomal RNA (rRNA) was examined by dual-primer extension assay. A depurination primer was used to measure the extent of rRNA depurination and the 28S rRNA primer was used to measure the total amount of 28S rRNA in the primer extension reaction. Ribosome depurination was observed after 6 h exposure to 0.1 μg/ml RTA and was maintained through12 h; however, ribosome depurination was decreased at 18 h (Fig. 17). No depurination was observed in untreated control cells.

Stx2 activates JNK and p38 signaling pathways in Vero cells

Stx2 activated JNK1, JNK2, and p38 signaling pathways within 2 h of treatment in Vero cells (Fig. 18). JNK activation was maintained through 6 h while p38 activation was decreased at 6 h. PARP is a DNA repair molecular and PARP cleavage is used as a marker of late-stage apoptosis. Stx2 did not induce PARP cleavage until 6 h of treatment.

Transfection of Stx induces apoptosis in Vero cells

In tobacco plants, co-expression of L3Δ99 with PAP prevented PAP-induced ribosome depurination (76). Since PAP and Stx are both ribosome inactivation proteins

targeting the same substrate, the ribosome, we investigated if co-expression of L3Δ99 with the A-chain of Stx1 or Stx2 could reduce the cytotoxicity induced by Stx in Vero cells. As shown in Fig. 19, bands were detected when cells were transfected with the different plasmids. A band that migrated close to the expected molecular weight of 11 kDa L3Δ99 was observed in cells transfected with L3Δ99 alone. A second band of higher MW was also observed, suggesting that the larger molecular weight band might be a dimmer. With transfection of Stx1a alone, a lower MW band was observed, but this was not the predicted size of Stx1a, suggesting that degradation of Stx1a may have occurred. With transfection of Stx2a alone, a faint band was observed at the correct size, though a higher band was also detected. When cells were co-transfected with L3Δ99 and Stx1a, the two bands of L3Δ99 and a single band of Stx1a were observed. Surprisingly, while three bands presented in co-transfection of L3Δ99 and Stx1a, two bands of L3Δ99 were not observed with co-transfection of L3Δ99 and stx2.

We next determined if transfection of these DNA plasmids induced caspase 3/7 activity. As shown in Fig. 20, transfection with either vector or L3Δ99 alone showed very low caspase-3/7 activity. Surprisingly, a low level of caspase-3/7 activity was also observed in Vero cells transfected with Stx1a. Transfection of Stx2a alone induced caspase-3/7 activity compare to vector or L3Δ99; however, co-transfection of L3Δ99 and

Stx2 showed a similar level of caspase-3/7 activity relative to Stx2a alone (Fig. 20). Collectively, our date suggest that co-expression of L3Δ99 and Stx2a did not prevent Vero cells from Stx-induced caspase-3/7.

While we had proposed that L3Δ99 might have a protective effect on Stx-induced apoptosis, L3Δ99 and Stx were transfected at the same time in Vero cells. Therefore, we examine the ability of exogenous Stx2 to induce apoptosis in Vero cells which were expressing L3Δ99. As shown in Fig. 21, exogenous Stx2-induced caspase-3/7 activities were similar in Vero cells in the presence or absence of L3Δ99; indicating expression of L3Δ99 did not inhibit Stx2-induced apoptosis.

Discussion

In the present study, we have investigated the effect of L3Δ99, a truncated fragment of the L3 ribosomal protein, on Stx-induced apoptosis. Expression of L3Δ99 did not inhibit Stx-induced apoptosis in Vero cells. Preliminary data from our collaborator showed that L3Δ99 conferred Stx-induced cytotoxicity in yeast (Tumer, unpublished); however, our results from a mammalian epithelial cell culture system did not correlate with their findings. Vero cells have been routinely used in our laboratory to examine the action of another RIP, ricin, and bioactivity of exogenous Stx2 was

demonstrated by caspase-3/7 activation, ribosome depurination, JNK pathway activation, p38 MAK pathway activation, and PARP cleavage. For the expression experiments, we have optimized the transfection conditions such as cell density, incubation time, and transfection reagent/DNA ratio. DNA quality was also assured to yield the highest transfection efficiency. However, we were experiencing difficulties in expressing L3Δ99, Stx1, and Stx2, as well as identifying them despite V5 tag. In the case of co-expression of L3Δ99 and Stx2, the expression of L3Δ99 and Stx2 were diminished compared to some level of expression of L3Δ99 or Stx2 alone.

Moreover, we have optimized the condition of co-expression of L3Δ99 with Stx1a or Stx2a which is the active subunit of Stx. L3Δ99 did not play a relevant role of Stx2-induced caspase-3/7 activation whether Vero cells were treated exogenously or transfected with Stx2. The limitation of the experiment is that we are not certain that the level of L3Δ99 is sufficient to cause bioactivity. The data from this study is inconclusive and needed to be investigated in depth to advance our knowledge of the Stx-induced apoptosis and the potential therapeutic interventions.

CHAPTER FOUR

CONCLUSIONS OF THE THESIS

The relationship between protein synthesis and cytotoxicity induced by ribosome-inactivating proteins (RIPs) in mammalian systems is still unclear. Our long-range goal is to investigate this relationship using recombinant ricin A-chain (RTA) mutants that are deficient in their ability to either inhibit protein synthesis or apoptosis. To be able to accomplish this goal, we have established a nontransformed epithelial cell culture system, MAC-T, that is sensitive to RTA in the absence of ricin B-chain. We have demonstrated that RTA alone induces apoptosis, depurinates ribosomes, inhibits protein synthesis, and activates MAPK pathways in MAC-T cells. Moreover, we have observed that the inhibition of the JNK pathway by chemical inhibitors or JNK2 siRNA reduces apoptosis induced by RTA. We also determined that the JNK pathway plays a major role in RTA-induced apoptosis in MAC-T cells. Additionally, Stx2 also induced apoptosis, depurinated ribosomes, and activated MAPK pathways in Vero cells. However, a truncated fragment of the L3 ribosomal protein did not play a relevant role in Stx-induced apoptosis. Knowledge of the relationship between ribosome depurination and apoptosis is important for developing treatments against RIP intoxication in mammalian systems.

Figures

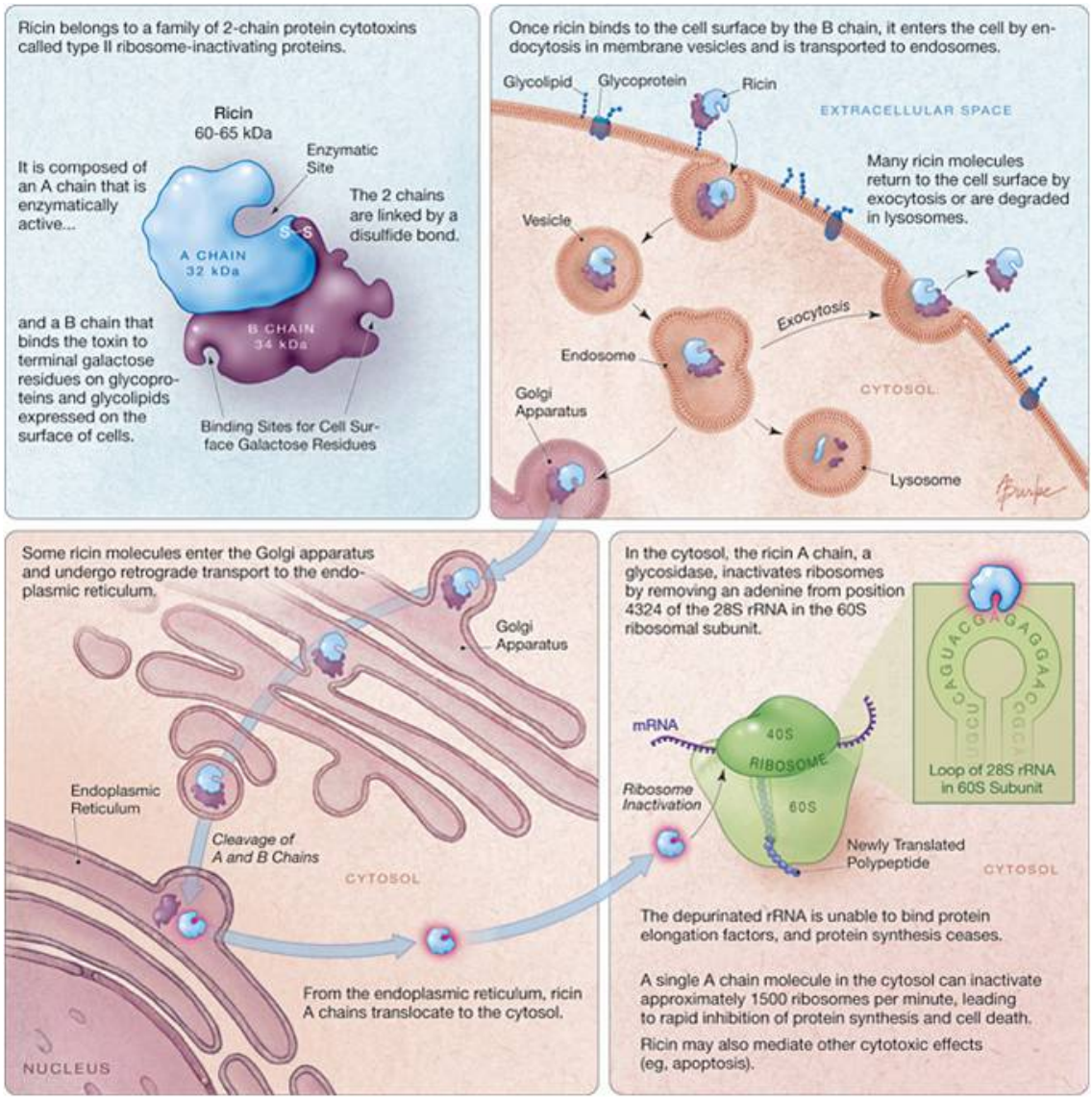

Figure 1. **Retrograde translocation of ricin.** From Audi et al., 2005 (1).

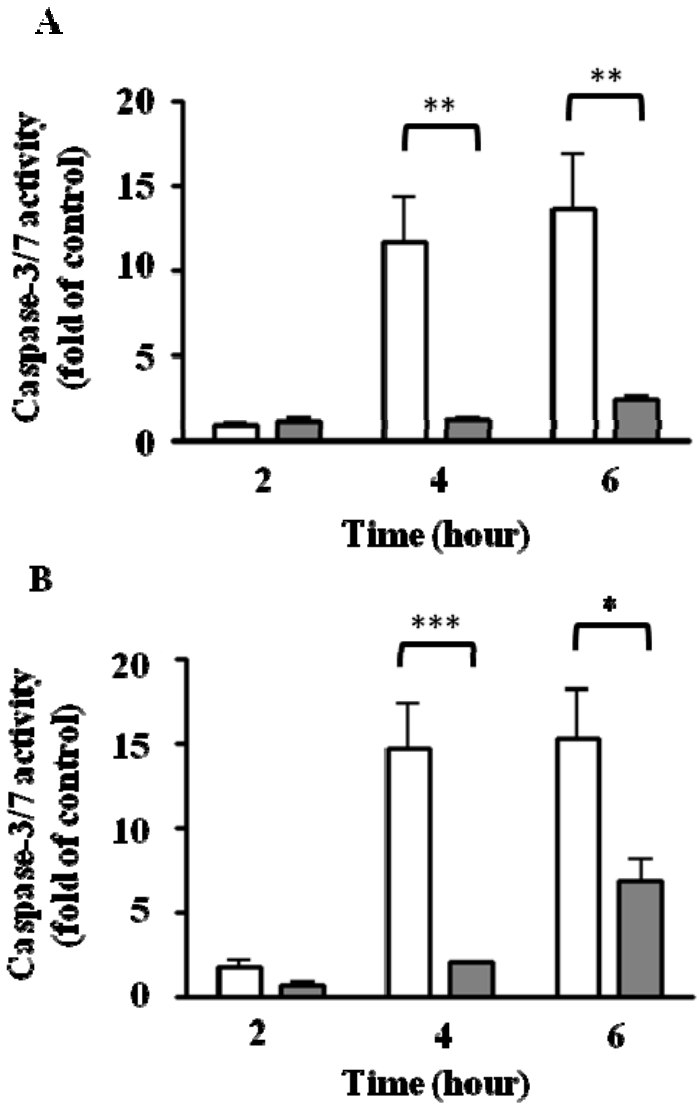

Figure 2. Comparison of RTA-induced caspase-3/7 activation in MAC-T, Vero and HeLa cells. (A) Confluent MAC-T (white bars) and Vero (gray bars) cells were serum-starved for 16 h prior to treatment with 1 μg/ml RTA for the indicated times. (B) Confluent MAC-T (white bars) and HeLa (gray bars) cells were serum-starved for 2 h prior to treatment with 1 μg/ml RTA for the indicated times. Apoptosis was measured using the fluorescent SensoLyte Homogeneous AMC Caspase 3/7 Assay kit (AnaSpec). Bars represent mean ± S.E. of three experiments. Data are relative to caspase 3/7 activity in the absence of RTA. Data were analyzed by two-way ANOVA with repeated measures with Bonferroni post-tests. *$P < 0.05$; **$P < 0.01$; ***$P < 0.001$ for Vero or HeLa cells vs. MAC-T cells. Adapted from Jetzt, Cheng, Tumer and Cohick; 2009 (81).

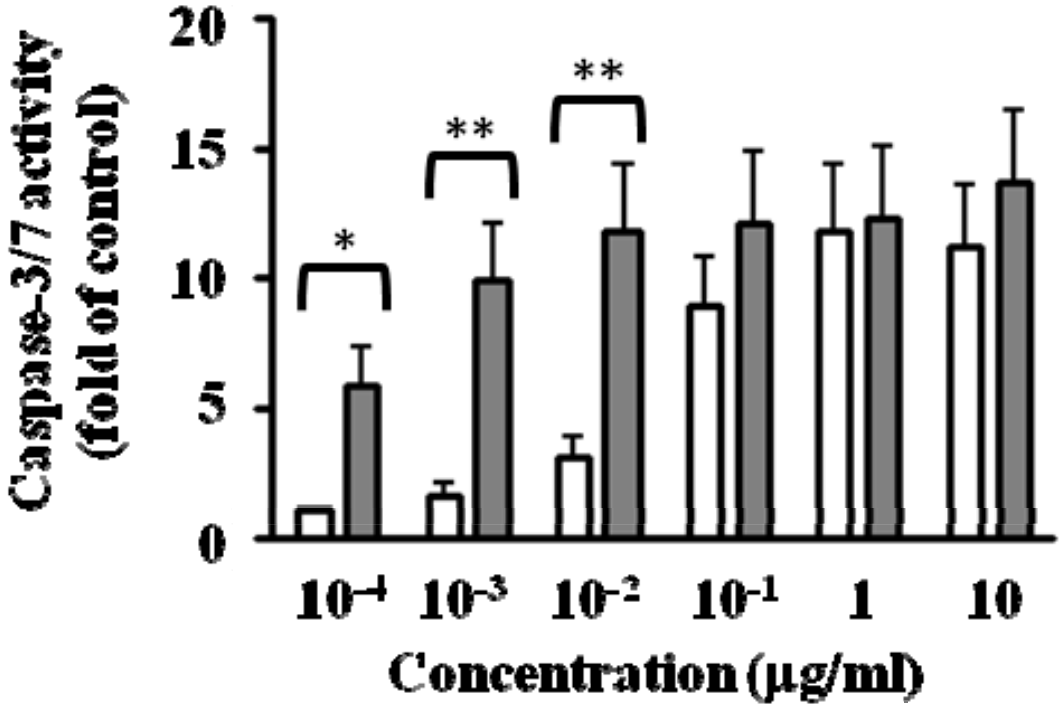

Figure 3. Comparison of RTA- and ricin holoenzyme-induced caspase-3/7 activation. Confluent MAC-T cells were serum-starved for 16 h before treatment with RTA or ricin holoenzyme for 6 h. Apoptosis was measured using the fluorescent SensoLyte Homogeneous AMC Caspase 3/7 Assay kit (AnaSpec). Bars represent mean ± S.E. of four experiments. Data are relative to caspase-3/7 activity in the absence of RTA. White bars, RTA; gray bars, ricin holoenzyme. Data were analyzed by two-way ANOVA with Bonferroni post-tests. *$P < 0.01$; **$P < 0.001$ for RTA vs. ricin holoenzyme. Adapted from Jetzt, Cheng, Tumer and Cohick; 2009 (81).

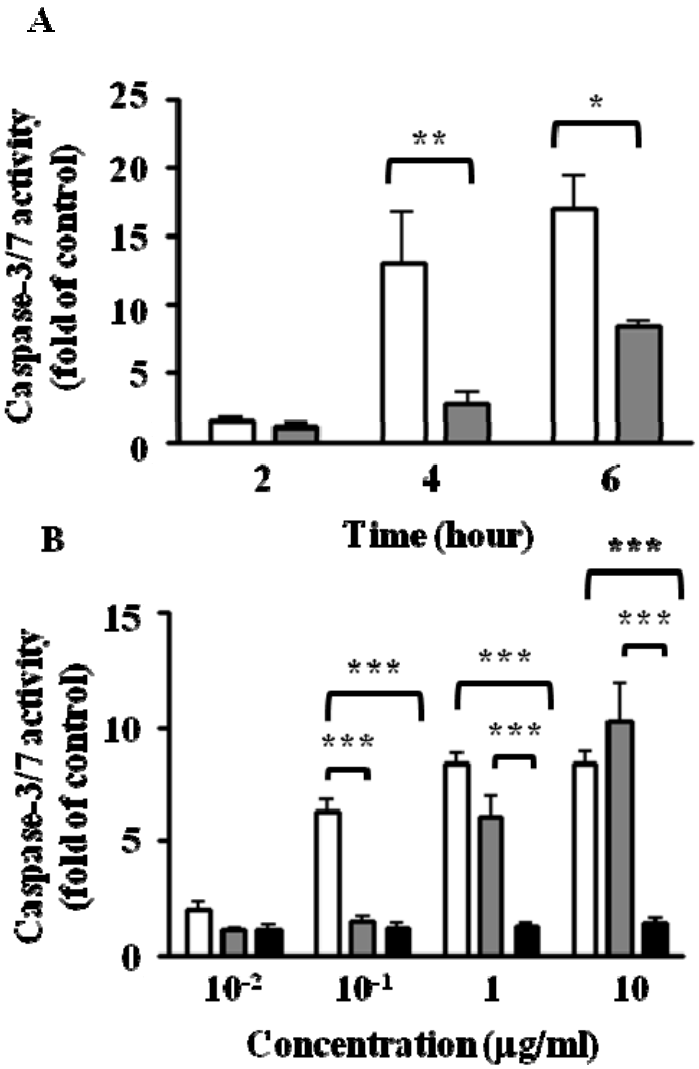

Figure 4. RTA obtained from Sigma induces caspase-3/7 activity more efficiently than RTA obtained from Vector Laboratories. (A) Time course of apoptotic response to RTA obtained from different suppliers. Confluent MAC-T cells were serum-starved for 16 h prior to treatment with 1 µg/ml RTA for the indicated times. RTA obtained from Sigma (white bars) or Vector Laboratories (gray bars). (B) Apoptotic response to increasing concentrations of RTA obtained from different suppliers, as well as RTB. Cells were serum-starved for 16 h prior to treatment with RTA from Sigma (white bars), RTA from Vector Laboratories (gray bars), or RTB (black bars) for 6 h. Apoptosis was measured using the fluorescent SensoLyte Homogeneous AMC Caspase 3/7 Assay kit (AnaSpec). Bars represent mean ± S.E. of at least three experiments. Data are relative to caspase 3/7 activity in untreated control cells. Data were analyzed by two-way ANOVA with repeated measures with Bonferroni post-tests. *$P < 0.05$; **$P < 0.01$; ***$P < 0.001$ for time (panel A) or concentration (panel B) comparisons.

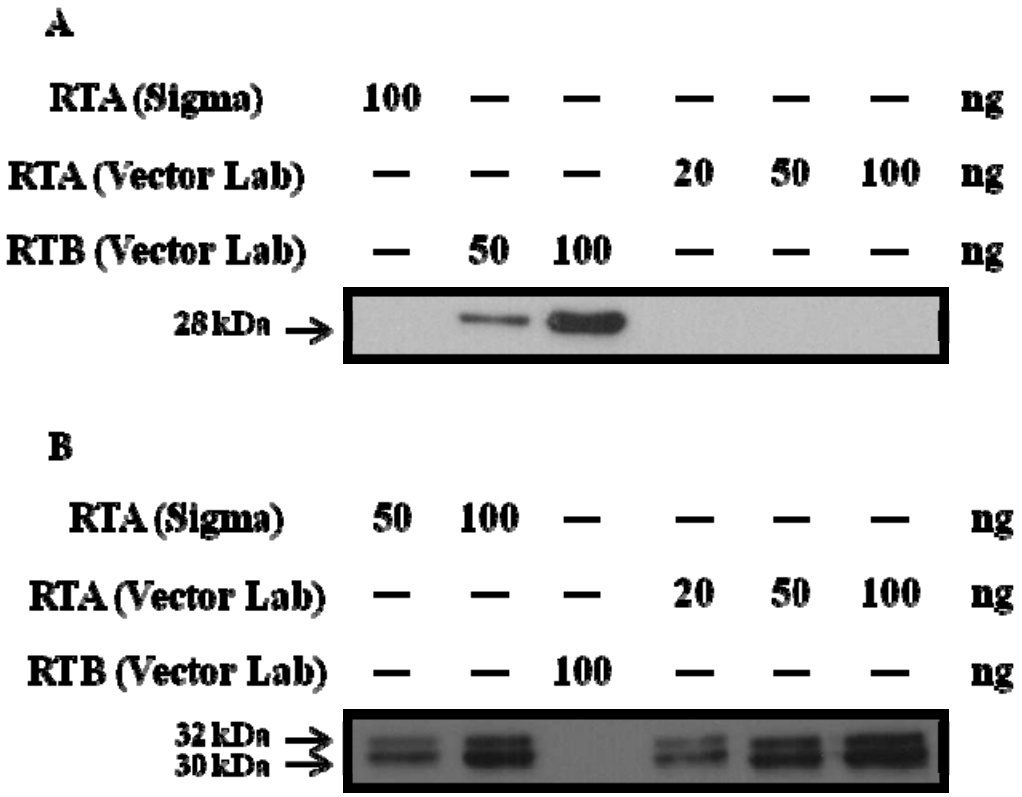

Figure 5. RTA is not contaminated with RTB regardless of source. RTA was separated by SDS-PAGE and immunoblotted with antibody against RTB (A) or RTA (B).

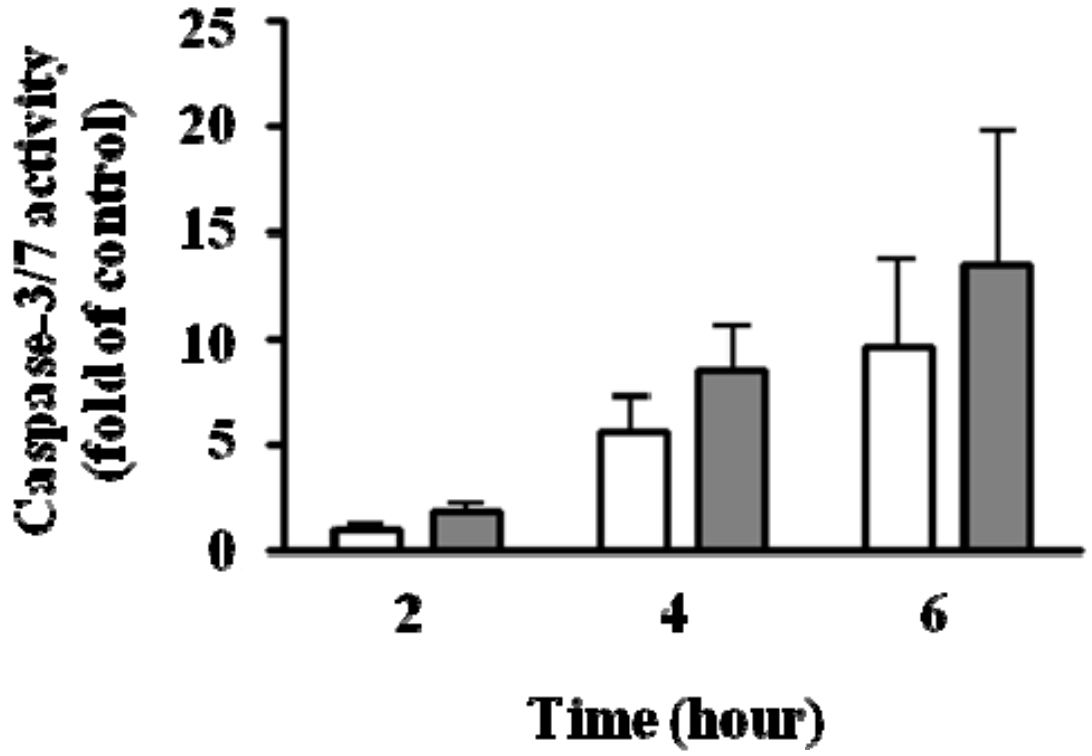

Figure 6. Effect of RTA on caspase-3/7 activation when cells are exposed to RTA for the first h of treatment compared to the entire time. Confluent MAC-T cells were serum-starved for 16 h prior to treatment with 1 μg/ml RTA for the indicated times. Apoptosis was measured using the fluorescent SensoLyte Homogeneous AMC Caspase-3/7 Assay kit (AnaSpec). White bars; RTA was removed after 1 h of treatment and replaced with SF media; gray bars, RTA remained in the culture media the entire treatment time. Bars represent mean ± S.E. of at least three experiments. Data are relative to caspase-3/7 activity in the absence of RTA. Data were analyzed by two-way ANOVA with repeated measures with Bonferroni post-tests.

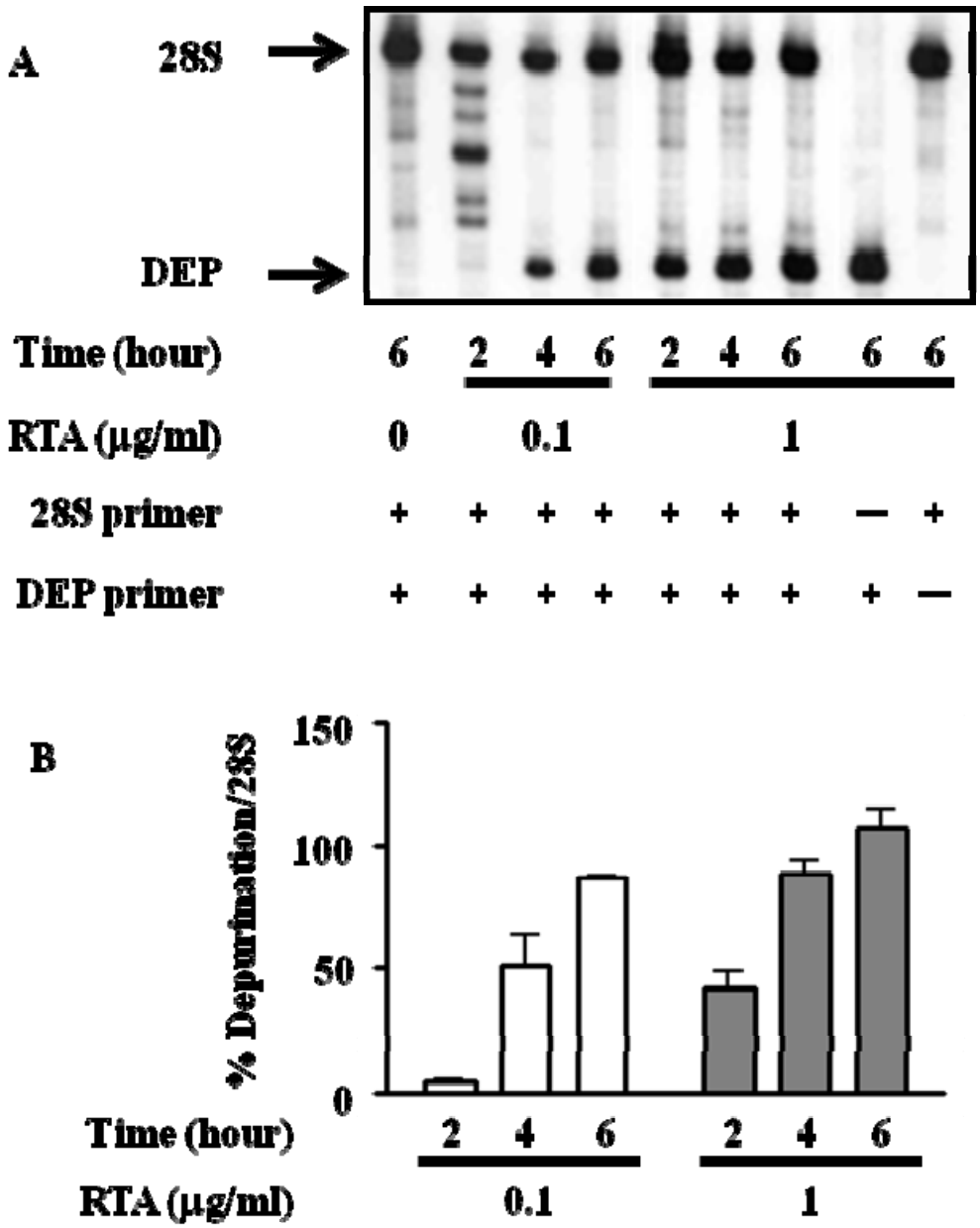

Figure 7. RTA induces ribosome depurination in a time- and concentration-dependent manner in MAC-T cells. (A) Confluent MAC-T cells were serum-deprived for 16 h prior to treatment with RTA for the indicated times. Total RNA was analyzed by a dual-primer extension assay with primers designed to recognize sequences downstream of the depurination site and the 5′ end of the bovine 28S ribosome. (B) Depurination was quantified and normalized against total 28S RNA. Bars represent mean ± S.D. of two experiments. Adapted from Jetzt, Cheng, Tumer and Cohick; 2009 (81).

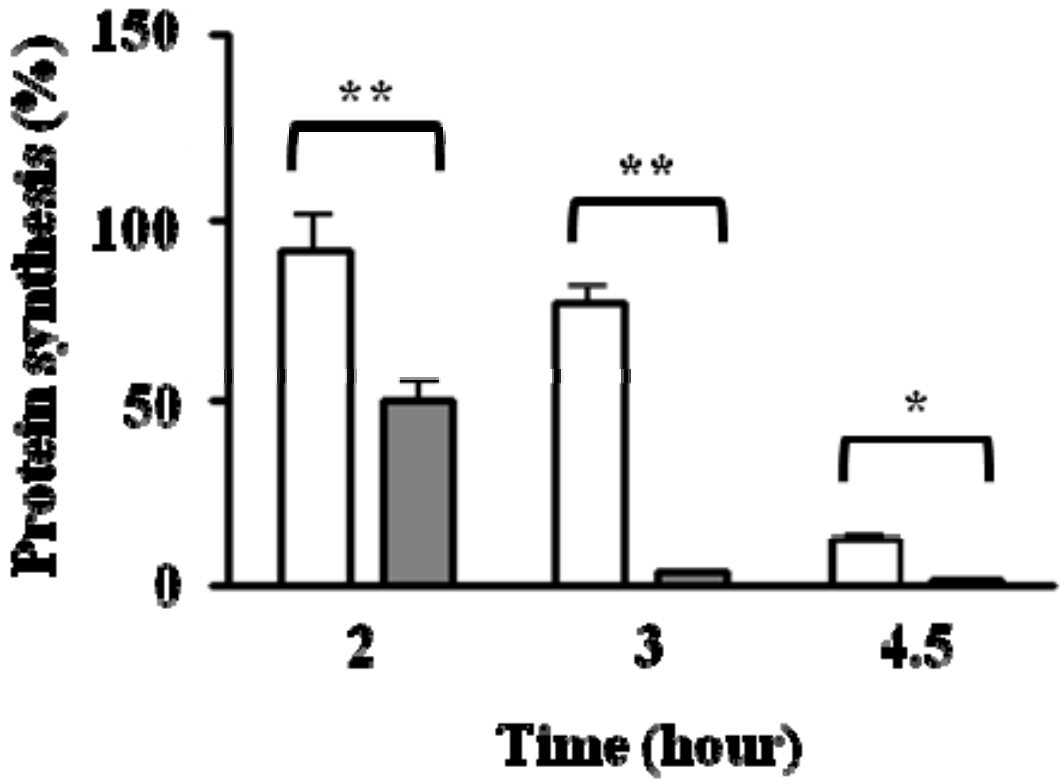

Figure 8. RTA inhibits protein synthesis in a time- and concentration-dependent manner. Confluent MAC-T cells were serum-starved for 16 h prior to incubation in methionine-free media for 45 min prior to treatment with RTA for the indicated times. [35S]methionine was added to cells during the last hour of RTA treatment. Total protein synthesis was determined by [35S]methionine incorporation. Bars represent mean ± S.E. of three experiments. White bars, 0.1 μg/ml RTA; gray bars, 1 μg/ml RTA. Data were analyzed by two-way repeated measures ANOVA with Bonferroni post-tests. *$P < 0.05$; **$P < 0.01$ for 0.1 μg/ml vs. 1.0 μg/ml RTA. Adapted from Jetzt, Cheng, Tumer and Cohick; 2009 (81).

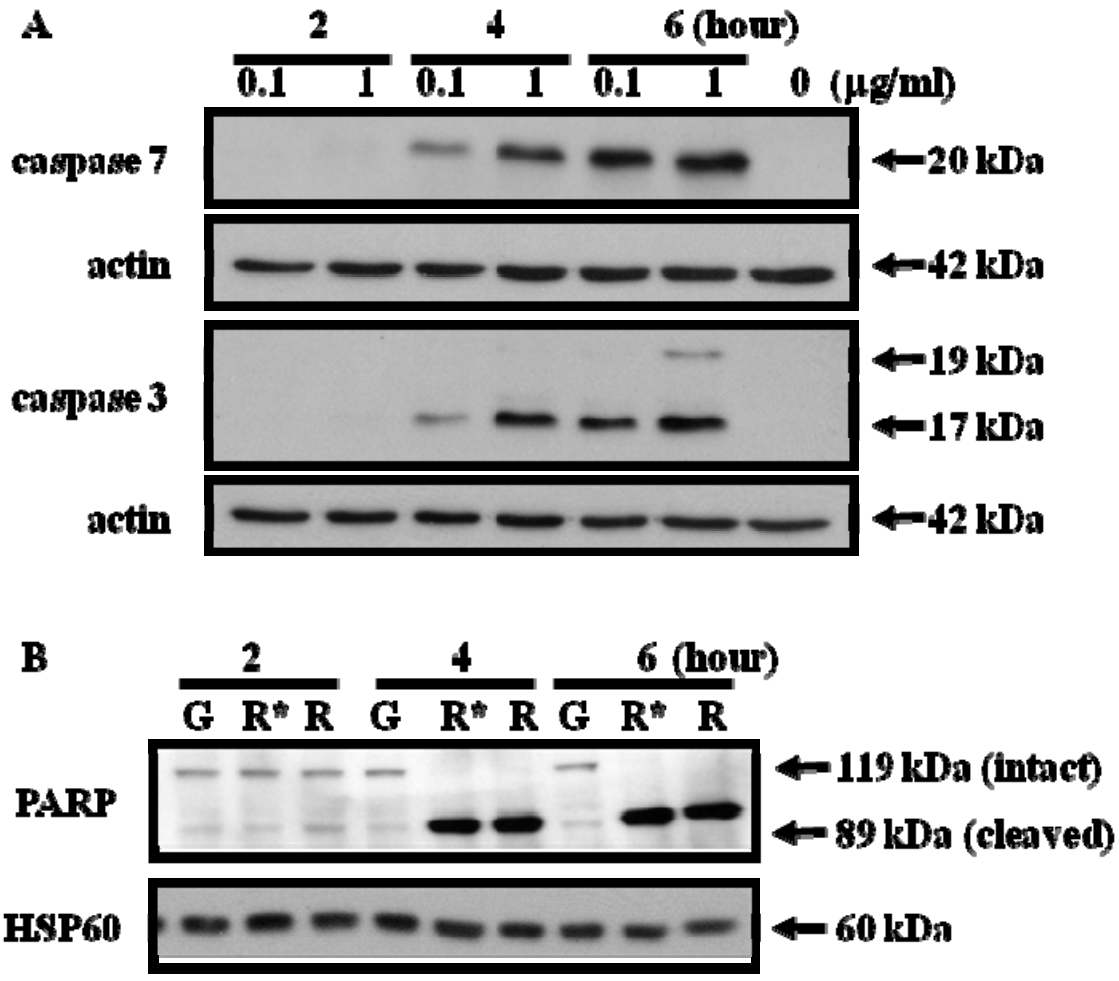

Figure 9. RTA induces cleavage of caspase-3/7 and PARP. (A) Confluent MAC-T cells were serum starved for 16 h prior to addition of glycerol (G) or RTA, 0.1 or 1 μg/ml for the indicated times. Cell lysates (30 μg total protein) were separated by SDS-PAGE and immunoblotted. Figure is representative of three separate experiments. (B) Cells were serum-starved for 18 h prior to addition of glycerol (G) or 1 μg/ml RTA (R*, RTA was removed after 1 h of treatment and replaced with SF media; R, RTA remained in the culture media the entire treatment time). Cell lysates (50 μg total protein) were separated by SDS-PAGE and immunoblotted. Bands at 119 and 89 kDa represent intact and cleaved PARP, respectively. Figure is representative of 2 separate experiments. The caspase 7 antibody recognizes the 20 kDa subunit, while the caspase 3 antibody recognizes two cleaved species; the 17 kDa subunit and the 19 kDa subunit which contains the prodomain. Adapted from Jetzt, Cheng, Tumer and Cohick; 2009 (81).

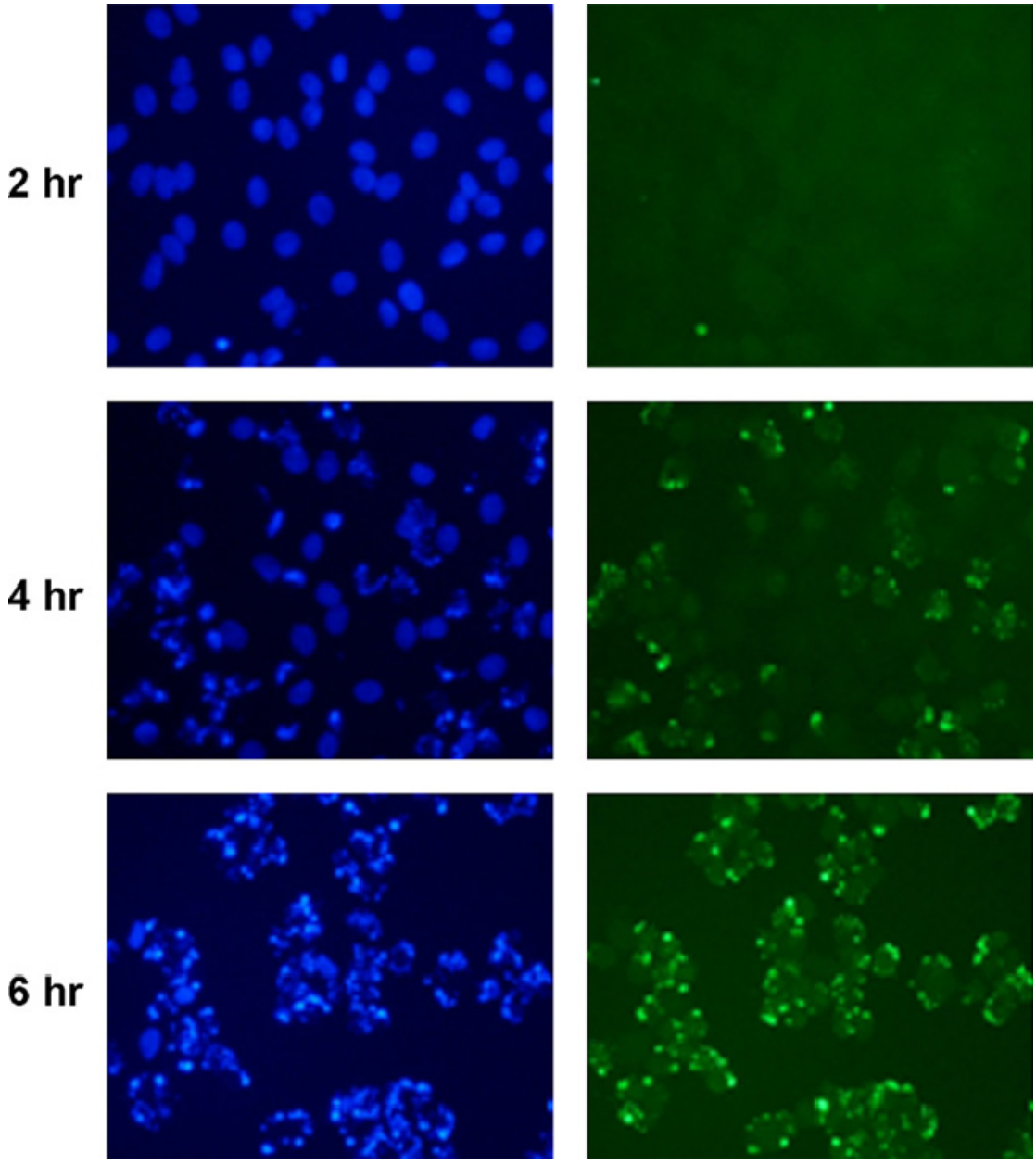

Figure 10. RTA induces TdT-mediated dUTP nick end labeling (TUNEL) staining in a time-dependent manner. MAC-T cells were plated on glass chamber slides and grown to confluence. Cells were serum-starved overnight and treated with 1 μg/ml RTA for 2, 4, and 6 h. Nuclei were stained with Hoechst 33342 (left panel), and ricin-induced DNA strand breaks were detected using TUNEL staining (right panel). Adapted from Jetzt, Cheng, Tumer and Cohick; 2009 (81).

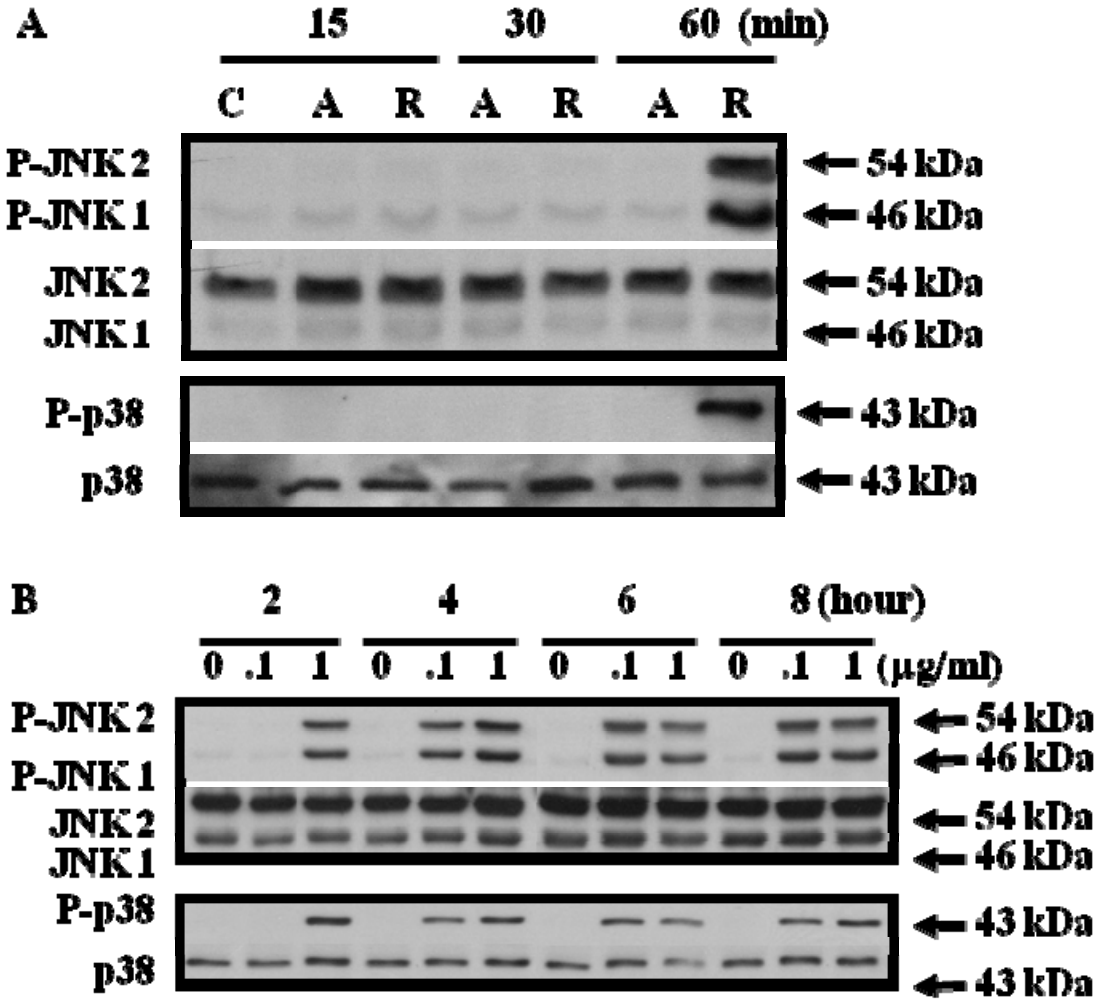

Figure 11. RTA and ricin holoenzyme activate JNK and p38 in MAC-T cells. (A) Confluent MAC-T cells were serum-starved for 16 h prior to treatment with glycerol (G), 1 μg/ml RTA (A) or ricin holoenzyme (R) for the indicated times. (B) Cells were serum starved for 16 h before treatment with 0.1 and 1μg/ml RTA for the indicated times. For each experiment, total cell lysates (30 μg) were immunoblotted with phospho-specific antibodies, then membranes were stripped and reprobed with antibodies for total protein. Blots are representative of 2–3 separate experiments. Adapted from Jetzt, Cheng, Tumer and Cohick; 2009 (81).

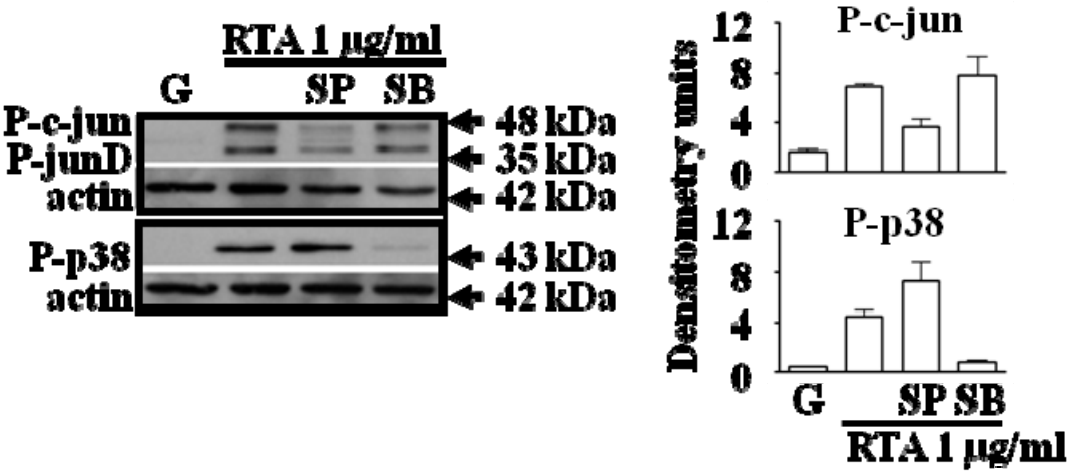

Figure 12. Chemical inhibitors inhibit the JNK and the p38 pathways. Confluent MAC-T cells were serum-starved for 16 h before treatment with RTA ± inhibitor for 4 h. Total cell lysates (30 µg) were separated by SDS-PAGE, immunoblotted and quantified by densitometry. Bars represent mean ± S.E. of three separate experiments. A representative blot is shown on the left. Adapted from Jetzt, Cheng, Tumer and Cohick; 2009 (81).

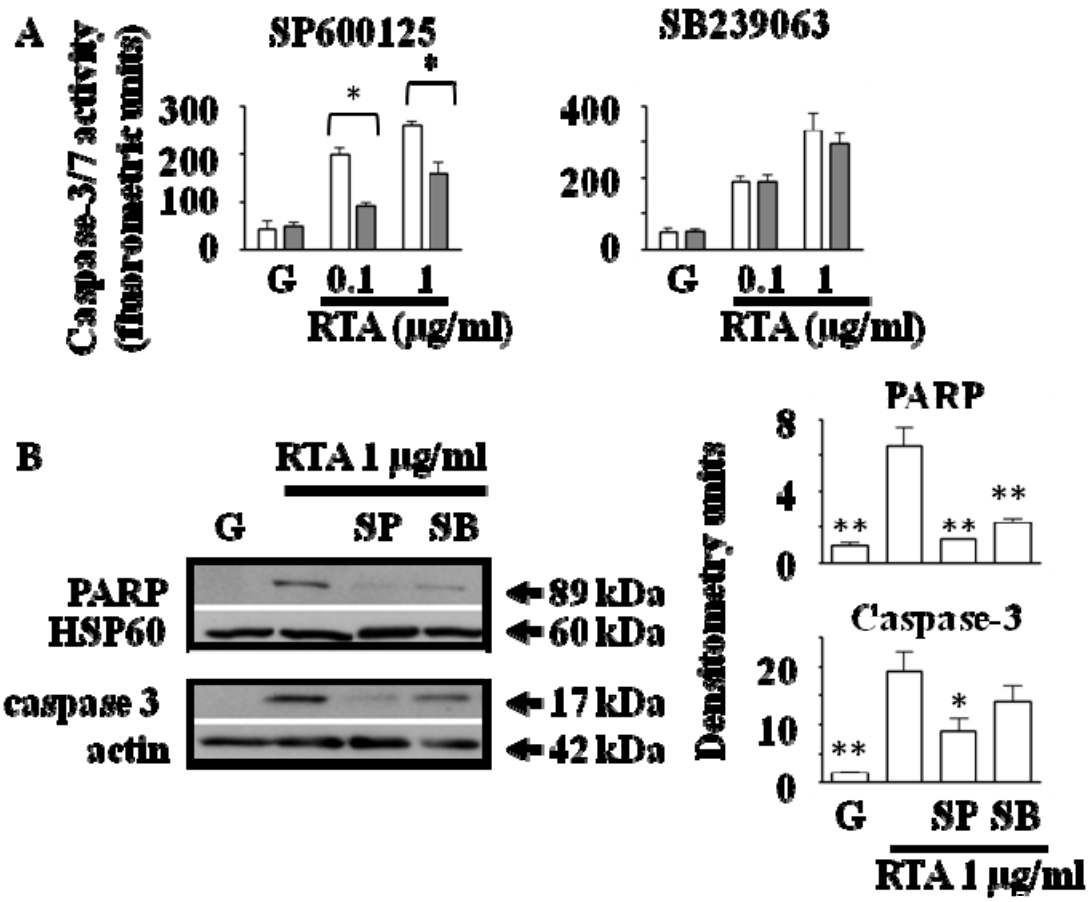

Figure 13. Effect of chemical inhibition of JNK1/2 and p38 signaling pathways on RTA-induced caspase activation and PARP cleavage. Confluent MAC-T cells were serum-starved for 16 h before treatment with RTA ± inhibitor for 4 h. (A) Apoptosis was measured using the fluorescent SensoLyte Homogeneous AMC Caspase 3/7 Assay kit (AnaSpec). Bars represent mean ± S.E. of three separate experiments for SP600125 (50 µM) and five separate experiments for SB239063 (30 µM). White bars, DMSO control; gray bars, inhibitor. Data were analyzed by two-way ANOVA with Bonferroni post-tests. *$P < 0.001$ for treatment with inhibitor vs. treatment without inhibitor. (B) Total cell lysates (30 µg) were separated by SDS-PAGE, immunoblotted, and quantified by densitometry. Bars represent mean ± S.E. of five separate experiments. Data were analyzed by one-way ANOVA with Dunnett's Multiple Comparison post-test. *$P < 0.05$; **$P < 0.01$; indicates difference from RTA alone. A representative blot is shown on the left. Adapted from Jetzt, Cheng, Tumer and Cohick; 2009 (81).

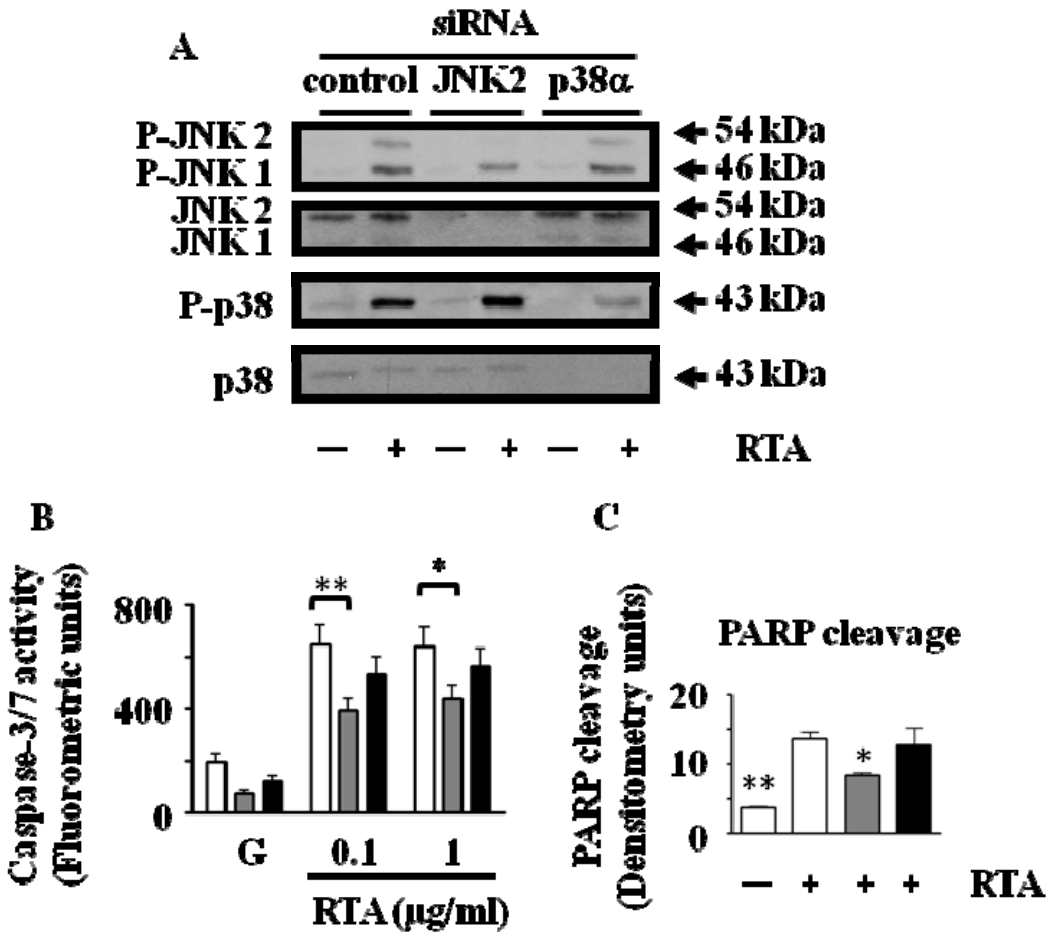

Figure 14. siRNA inhibition of JNK2 but not p38α decreases RTA-induced caspase 3/7 activation and PARP cleavage. MAC-T cells were transfected with siRNA and treated with 1 μg/ml RTA for 4 or 6 h. (A) Total cell lysates were separated by SDS-PAGE and immunoblotted. Blots are representative of two separate experiments. (B) Apoptosis was measured using the fluorescent SensoLyte Homogeneous AMC Caspase 3/7 Assay kit (AnaSpec). Bars represent mean ± S.E. of six separate experiments. Data were analyzed by two-way ANOVA with Bonferroni post-tests. *$P < 0.05$; **$P < 0.01$; NS = $P > 0.05$. (C) Immunoblots probed with PARP antibody were quantfied by densitometry and normalized using HSP60. White bars, scramble control; gray bars, JNK2 siRNA; black bars, p38α siRNA. Bars represent the mean ± S.E. of three separate experiments. Data were analyzed by one-way ANOVA with Dunnett's Multiple Comparison post-tests. *$P < 0.05$; **$P < 0.01$; indicates difference from RTA alone. Adapted from Jetzt, Cheng, Tumer and Cohick; 2009 (81).

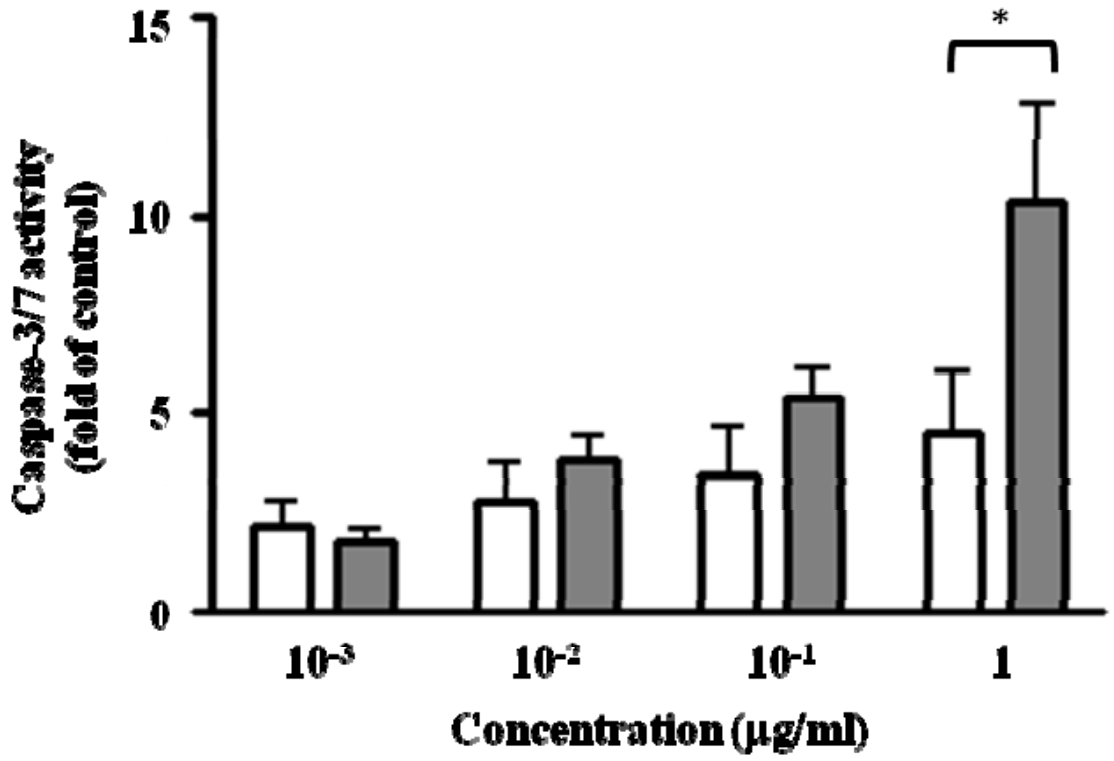

Figure 15. Comparison of Stx2-induced caspase-3/7 cleavage in HeLa and Vero cells. Confluent HeLa (white bars) and Vero (gray bars) cells were serum-starved for 2 h prior to treatment with Stx2 for 6 h. Apoptosis was measured using the fluorescent SensoLyte Homogeneous AMC Caspase 3/7 Assay kit (AnaSpec). Bars represent mean ± S.E. of three experiments. Data are relative to caspase 3/7 activity in the absence of Stx2. Data were analyzed by two-way ANOVA with repeated measures with Bonferroni post-tests. *$P < 0.05$; for HeLa vs. Vero cells.

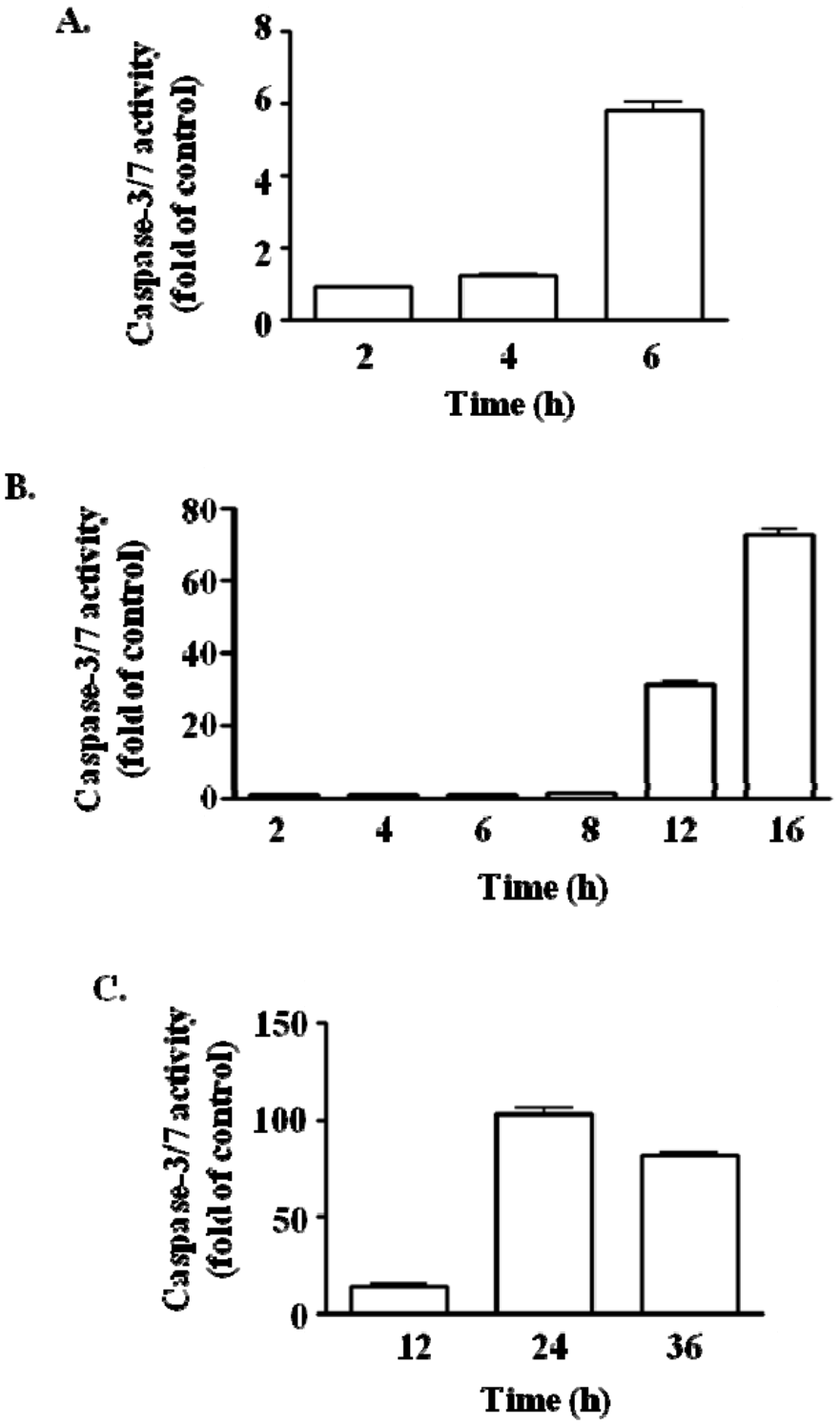

Figure 16. Effect of Stx2 on caspase-3/7 activation in Vero cells. Confluent Vero cells were serum-starved for 2 h prior to treatment with 0.1 μg/ml Stx2 for the indicated times. Apoptosis was measured using the fluorescent SensoLyte Homogeneous AMC Caspase 3/7 Assay kit (AnaSpec). Bars represent mean ± SD of triplicates in one experiment.

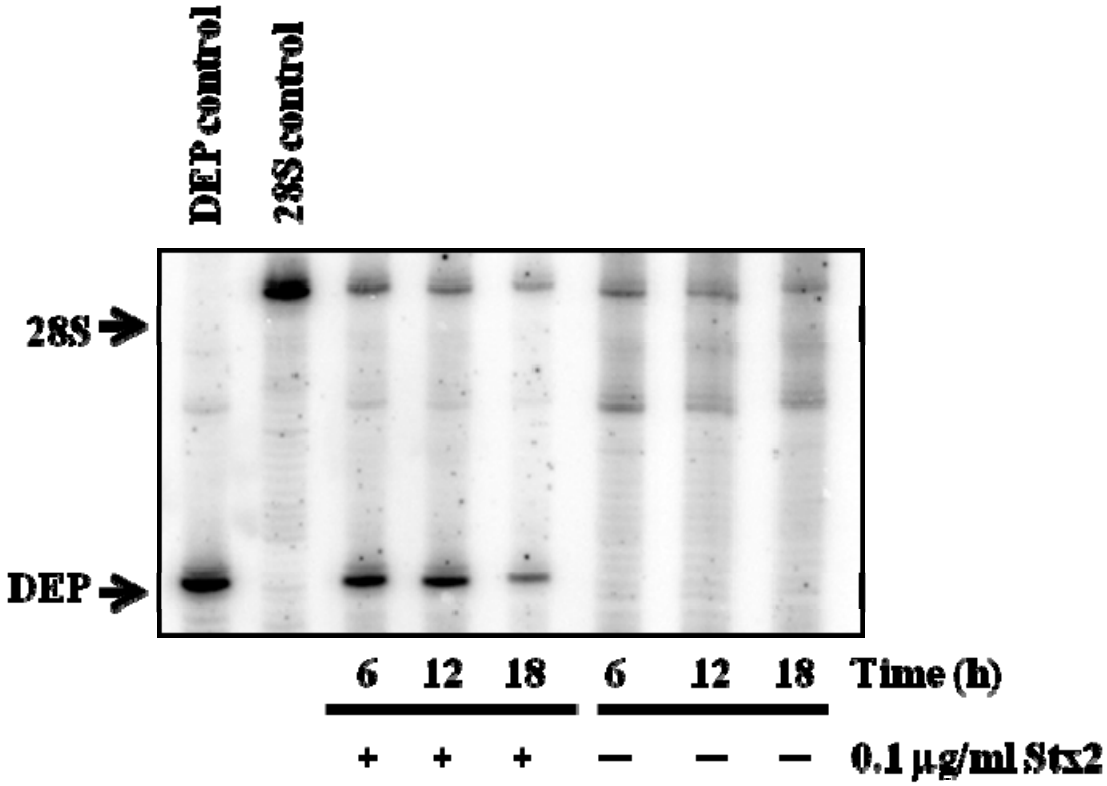

Figure 17. Effect of Stx2 on depurination in Vero cells. Confluent Vero cells were serum-deprived for 2 h prior to treatment with 0.1 µg/ml RTA for the indicated times. Total RNA was analyzed by a dual-primer extension assay with primers designed to recognize sequences downstream of the depurination site and the 5′ end of the 28S ribosome.

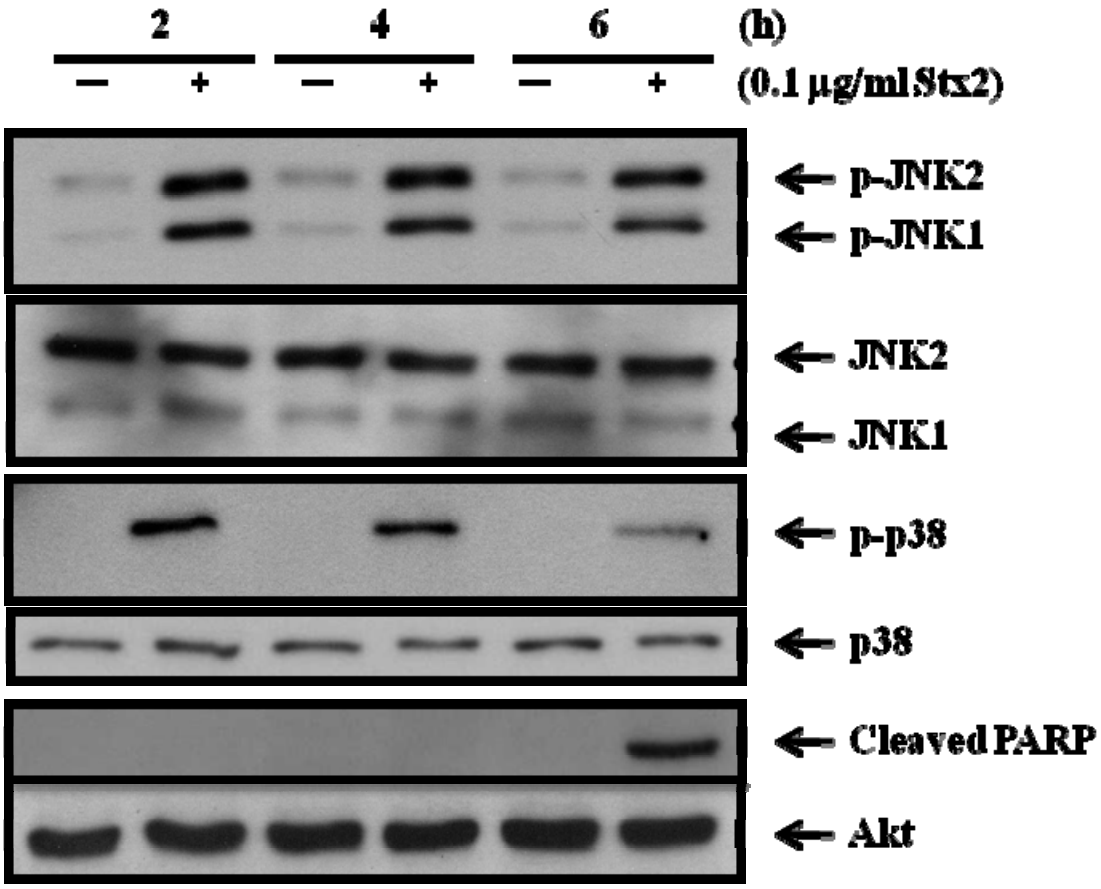

Figure 18. Stx2 activates JNK, p38, and PARP cleavage in Vero cells. Confluent Vero cells were serum-starved for 2 h prior to treatment with 0.1 μg/ml Stx2 for the indicated times. For each experiment, total cell lysates (30 μg) were immunoblotted with phospho-specific antibodies, then membranes were stripped, and reprobed with antibodies for total protein. Blots are representative of two separate experiments.

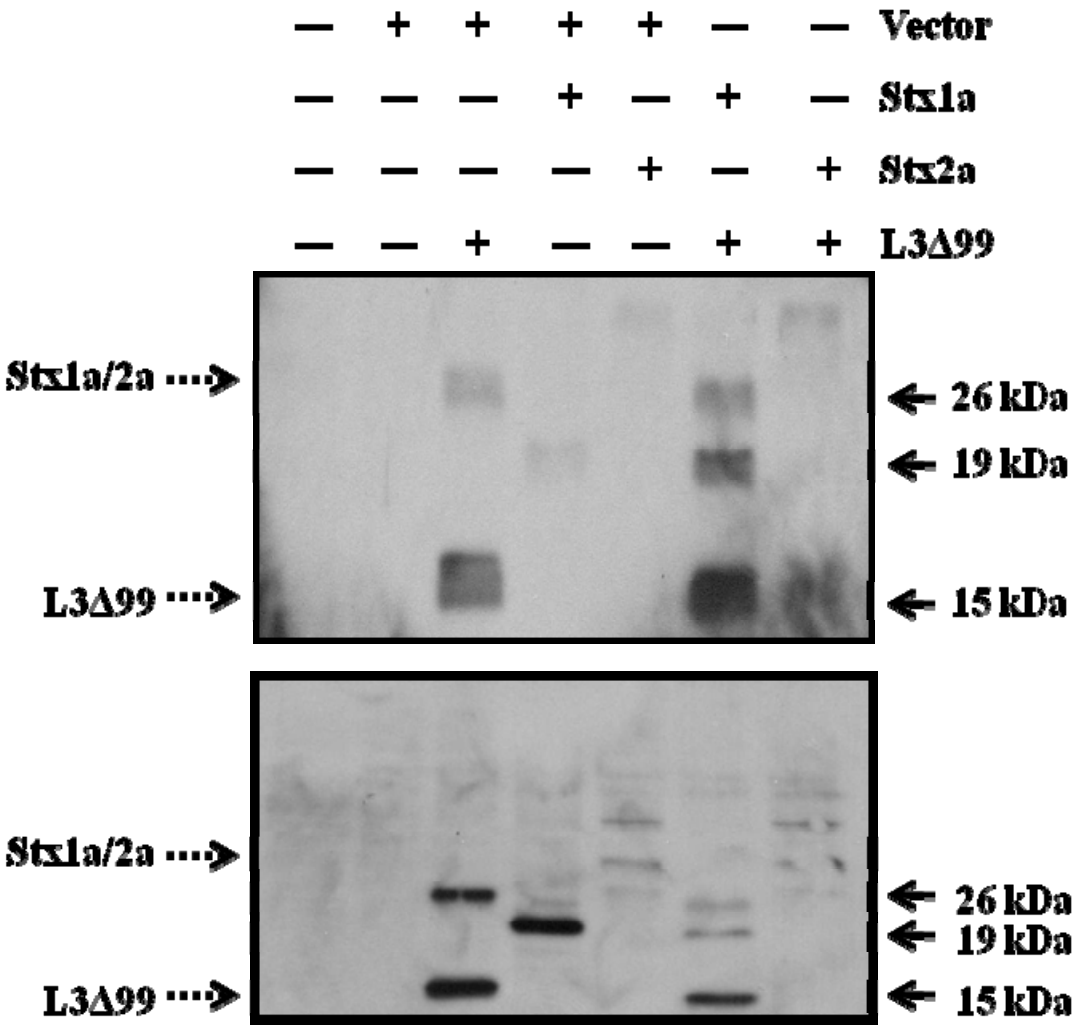

Figure 19. Co-expression of L3Δ99, Stx1a, or Stx2a in Vero cells. Vero cells were transfected with DNA codins for V5 tagged-L3Δ99, Stx1a, or Stx2a using Turbofect (Fermentas) according to manufacturer's protocol. Total cell lysates (30 µg) were separated by SDS-PAGE and immunoblotted with V5 antibody. Blots shown are two separate experiments.

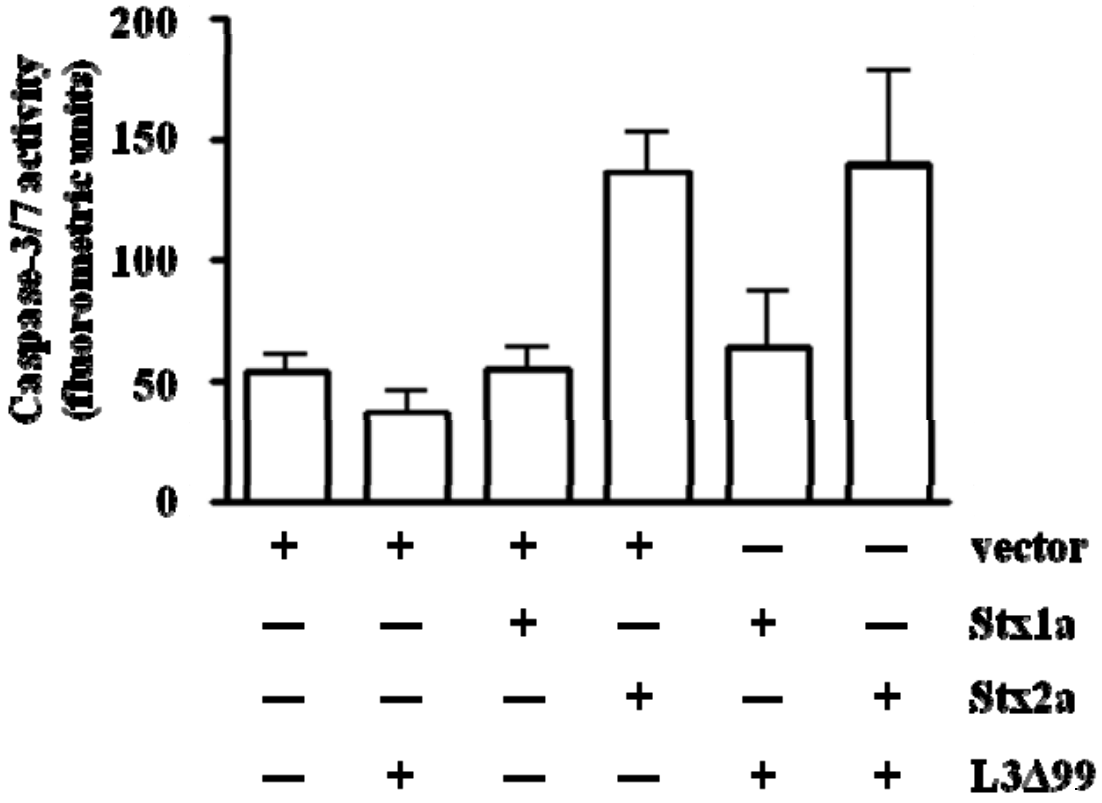

Figure 20. Effect of co-expression of Stx A-chain and L3Δ99 on caspase-3/7 activity in Vero cells. Vero cells were transfected with plasmid DNA using Turbofect (Fermentas) according to manufacturer's protocol. Apoptosis was measured using the fluorescent SensoLyte Homogeneous AMC Caspase-3/7 Assay (AnaSpec). Bars represent mean ± S.E. of 5 experiments.

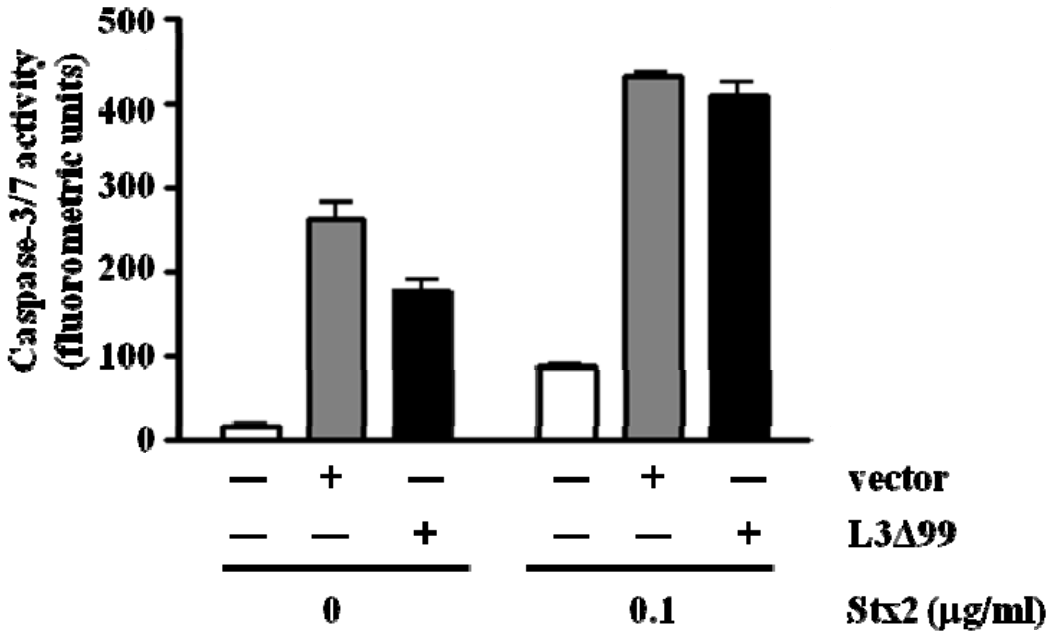

Figure 21. Effect of L3Δ99 expression on Stx2 with caspase-3/7 activity in Vero cells. Vero cells were transfected with DNA using Turbofect (Fermentas) according to manufacturer's protocol and treated with Stx2 for 6 h. Apoptosis was measured using the fluorescent SensoLyte Homogeneous AMC Caspase-3/7 Assay (AnaSpec). Bars represent triplicates of one experiment.

REFERENCES

1. **Audi J, Belson M, Patel M, Schier J, Osterloh J** 2005 Ricin poisoning: a comprehensive review. Jama 294:2342-2351
2. **Burdock GA, Carabin IG, Griffiths JC** 2006 Toxicology and pharmacology of sodium ricinoleate. Food Chem Toxicol 44:1689-1698
3. **Jackson LS, Zhang Z, Tolleson WH** Thermal stability of ricin in orange and apple juices. J Food Sci 75:T65-71
4. **Endo Y, Tsurugi K** 1988 The RNA N-glycosidase activity of ricin A-chain. Nucleic Acids Symp Ser:139-142
5. **Robertus JD, Yan X, Ernst S, Monzingo A, Worley S, Day P, Hollis T, Svinth M** 1996 Structural analysis of ricin and implications for inhibitor design. Toxicon 34:1325-1334
6. **Despeyroux D, Walker N, Pearce M, Fisher M, McDonnell M, Bailey SC, Griffiths GD, Watts P** 2000 Characterization of ricin heterogeneity by electrospray mass spectrometry, capillary electrophoresis, and resonant mirror. Anal Biochem 279:23-36
7. **Watson P, Spooner RA** 2006 Toxin entry and trafficking in mammalian cells. Adv Drug Deliv Rev 58:1581-1596
8. **Chen A, AbuJarour RJ, Draper RK** 2003 Evidence that the transport of ricin to the cytoplasm is independent of both Rab6A and COPI. J Cell Sci 116:3503-3510
9. **Liu Q, Zhan J, Chen X, Zheng S** 2006 Ricin A chain reaches the endoplasmic reticulum after endocytosis. Biochem Biophys Res Commun 343:857-863
10. **Bradberry SM, Dickers KJ, Rice P, Griffiths GD, Vale JA** 2003 Ricin poisoning. Toxicol Rev 22:65-70
11. **Coopman V, De Leeuw M, Cordonnier J, Jacobs W** 2009 Suicidal death after injection of a castor bean extract (Ricinus communis L.). Forensic Sci Int 189:e13-20
12. **Griffiths GD, Phillips GJ, Holley J** 2007 Inhalation toxicology of ricin preparations: animal models, prophylactic and therapeutic approaches to protection. Inhal Toxicol 19:873-887
13. **Vitetta ES, Smallshaw JE, Coleman E, Jafri H, Foster C, Munford R, Schindler J** 2006 A pilot clinical trial of a recombinant ricin vaccine in normal humans. Proc Natl Acad Sci U S A 103:2268-2273

14. **Smallshaw JE, Vitetta ES** A lyophilized formulation of RiVax, a recombinant ricin subunit vaccine, retains immunogenicity. Vaccine
15. **Marconescu PS, Smallshaw JE, Pop LM, Ruback SL, Vitetta ES** Intradermal administration of RiVax protects mice from mucosal and systemic ricin intoxication. Vaccine
16. **Stechmann B, Bai SK, Gobbo E, Lopez R, Merer G, Pinchard S, Panigai L, Tenza D, Raposo G, Beaumelle B, Sauvaire D, Gillet D, Johannes L, Barbier J** Inhibition of retrograde transport protects mice from lethal ricin challenge. Cell 141:231-242
17. **Wahome PG, Bai Y, Neal LM, Robertus JD, Mantis NJ** Identification of small-molecule inhibitors of ricin and shiga toxin using a cell-based high-throughput screen. Toxicon
18. **Bai Y, Monzingo AF, Robertus JD** 2009 The X-ray structure of ricin A chain with a novel inhibitor. Arch Biochem Biophys 483:23-28
19. **Lord JM, Roberts LM, Lencer WI** 2005 Entry of protein toxins into mammalian cells by crossing the endoplasmic reticulum membrane: co-opting basic mechanisms of endoplasmic reticulum-associated degradation. Curr Top Microbiol Immunol 300:149-168
20. **Korennykh AV, Correll CC, Piccirilli JA** 2007 Evidence for the importance of electrostatics in the function of two distinct families of ribosome inactivating toxins. Rna 13:1391-1396
21. **Olsnes S, Fernandez-Puentes C, Carrasco L, Vazquez D** 1975 Ribosome inactivation by the toxic lectins abrin and ricin. Kinetics of the enzymic activity of the toxin A-chains. Eur J Biochem 60:281-288
22. **Montanaro L, Sperti S, Mattioli A, Testoni G, Stirpe F** 1975 Inhibition by ricin of protein synthesis in vitro. Inhibition of the binding of elongation factor 2 and of adenosine diphosphate-ribosylated elongation factor 2 to ribosomes. Biochem J 146:127-131
23. **Osborn RW, Hartley MR** 1990 Dual effects of the ricin A chain on protein synthesis in rabbit reticulocyte lysate. Inhibition of initiation and translocation. Eur J Biochem 193:401-407
24. **Sandvig K, van Deurs B** 1992 Toxin-induced cell lysis: protection by 3-methyladenine and cycloheximide. Exp Cell Res 200:253-262
25. **Li XP, Baricevic M, Saidasan H, Tumer NE** 2007 Ribosome depurination is not sufficient for ricin-mediated cell death in Saccharomyces cerevisiae. Infect Immun 75:417-428

26. **Iordanov MS, Magun BE** 1999 Different mechanisms of c-Jun NH(2)-terminal kinase-1 (JNK1) activation by ultraviolet-B radiation and by oxidative stressors. J Biol Chem 274:25801-25806
27. **Iordanov MS, Pribnow D, Magun JL, Dinh TH, Pearson JA, Chen SL, Magun BE** 1997 Ribotoxic stress response: activation of the stress-activated protein kinase JNK1 by inhibitors of the peptidyl transferase reaction and by sequence-specific RNA damage to the alpha-sarcin/ricin loop in the 28S rRNA. Mol Cell Biol 17:3373-3381
28. **Higuchi S, Tamura T, Oda T** 2003 Cross-talk between the pathways leading to the induction of apoptosis and the secretion of tumor necrosis factor-alpha in ricin-treated RAW 264.7 cells. J Biochem 134:927-933
29. **Gonzalez TV, Farrant SA, Mantis NJ** 2006 Ricin induces IL-8 secretion from human monocyte/macrophages by activating the p38 MAP kinase pathway. Mol Immunol 43:1920-1923
30. **Korcheva V, Wong J, Corless C, Iordanov M, Magun B** 2005 Administration of ricin induces a severe inflammatory response via nonredundant stimulation of ERK, JNK, and P38 MAPK and provides a mouse model of hemolytic uremic syndrome. Am J Pathol 166:323-339
31. **Griffiths GD, Leek MD, Gee DJ** 1987 The toxic plant proteins ricin and abrin induce apoptotic changes in mammalian lymphoid tissues and intestine. J Pathol 151:221-229
32. **Korcheva V, Wong J, Lindauer M, Jacoby DB, Iordanov MS, Magun B** 2007 Role of apoptotic signaling pathways in regulation of inflammatory responses to ricin in primary murine macrophages. Mol Immunol 44:2761-2771
33. **Tamura T, Sadakata N, Oda T, Muramatsu T** 2002 Role of zinc ions in ricin-induced apoptosis in U937 cells. Toxicol Lett 132:141-151
34. **Rao PV, Jayaraj R, Bhaskar AS, Kumar O, Bhattacharya R, Saxena P, Dash PK, Vijayaraghavan R** 2005 Mechanism of ricin-induced apoptosis in human cervical cancer cells. Biochem Pharmacol 69:855-865
35. **Hu R, Zhai Q, Liu W, Liu X** 2001 An insight into the mechanism of cytotoxicity of ricin to hepatoma cell: roles of Bcl-2 family proteins, caspases, Ca(2+)-dependent proteases and protein kinase C. J Cell Biochem 81:583-593
36. **Stirpe F, Battelli MG** 2006 Ribosome-inactivating proteins: progress and problems. Cell Mol Life Sci 63:1850-1866
37. **Baluna R, Coleman E, Jones C, Ghetie V, Vitetta ES** 2000 The effect of a monoclonal antibody coupled to ricin A chain-derived peptides on endothelial

cells in vitro: insights into toxin-mediated vascular damage. Exp Cell Res 258:417-424

38. **Casellas P, Bourrie BJ, Gros P, Jansen FK** 1984 Kinetics of cytotoxicity induced by immunotoxins. Enhancement by lysosomotropic amines and carboxylic ionophores. J Biol Chem 259:9359-9364
39. **Lindstrom AL, Erlandsen SL, Kersey JH, Pennell CA** 1997 An in vitro model for toxin-mediated vascular leak syndrome: ricin toxin A chain increases the permeability of human endothelial cell monolayers. Blood 90:2323-2334
40. **Endo Y, Tsurugi K, Yutsudo T, Takeda Y, Ogasawara T, Igarashi K** 1988 Site of action of a Vero toxin (VT2) from Escherichia coli O157:H7 and of Shiga toxin on eukaryotic ribosomes. RNA N-glycosidase activity of the toxins. Eur J Biochem 171:45-50
41. **Waddell T, Head S, Petric M, Cohen A, Lingwood C** 1988 Globotriosyl ceramide is specifically recognized by the Escherichia coli verocytotoxin 2. Biochem Biophys Res Commun 152:674-679
42. **Sandvig K** 2001 Shiga toxins. Toxicon 39:1629-1635
43. **Ching JC, Jones NL, Ceponis PJ, Karmali MA, Sherman PM** 2002 Escherichia coli shiga-like toxins induce apoptosis and cleavage of poly(ADP-ribose) polymerase via in vitro activation of caspases. Infect Immun 70:4669-4677
44. **Keenan KP, Sharpnack DD, Collins H, Formal SB, O'Brien AD** 1986 Morphologic evaluation of the effects of Shiga toxin and E coli Shiga-like toxin on the rabbit intestine. Am J Pathol 125:69-80
45. **Muthing J, Schweppe CH, Karch H, Friedrich AW** 2009 Shiga toxins, glycosphingolipid diversity, and endothelial cell injury. Thromb Haemost 101:252-264
46. **Sandvig K, van Deurs B** 2005 Delivery into cells: lessons learned from plant and bacterial toxins. Gene Ther 12:865-872
47. **Lauvrak SU, Walchli S, Iversen TG, Slagsvold HH, Torgersen ML, Spilsberg B, Sandvig K** 2006 Shiga toxin regulates its entry in a Syk-dependent manner. Mol Biol Cell 17:1096-1109
48. **Ikeda M, Gunji Y, Yamasaki S, Takeda Y** 2000 Shiga toxin activates p38 MAP kinase through cellular Ca(2+) increase in Vero cells. FEBS Lett 485:94-98
49. **Cherla RP, Lee SY, Mees PL, Tesh VL** 2006 Shiga toxin 1-induced cytokine production is mediated by MAP kinase pathways and translation initiation factor eIF4E in the macrophage-like THP-1 cell line. J Leukoc Biol 79:397-407

50. **Walchli S, Skanland SS, Gregers TF, Lauvrak SU, Torgersen ML, Ying M, Kuroda S, Maturana A, Sandvig K** 2008 The Mitogen-activated protein kinase p38 links Shiga Toxin-dependent signaling and trafficking. Mol Biol Cell 19:95-104
51. **Jandhyala DM, Ahluwalia A, Obrig T, Thorpe CM** 2008 ZAK: a MAP3Kinase that transduces Shiga toxin- and ricin-induced proinflammatory cytokine expression. Cell Microbiol 10:1468-1477
52. **Olsnes S, Pihl A** 1972 Ricin - a potent inhibitor of protein synthesis. FEBS Lett 20:327-329
53. **Olsnes S, Pihl A** 1973 Different biological properties of the two constituent peptide chains of ricin, a toxic protein inhibiting protein synthesis. Biochemistry 12:3121-3126
54. **Hazes B, Read RJ** 1997 Accumulating evidence suggests that several AB-toxins subvert the endoplasmic reticulum-associated protein degradation pathway to enter target cells. Biochemistry 36:11051-11054
55. **Endo Y, Tsurugi K** 1988 The RNA N-glycosidase activity of ricin A-chain. The characteristics of the enzymatic activity of ricin A-chain with ribosomes and with rRNA. J Biol Chem 263:8735-8739
56. **Sikriwal D, Ghosh P, Batra JK** 2008 Ribosome inactivating protein saporin induces apoptosis through mitochondrial cascade, independent of translation inhibition. Int J Biochem Cell Biol 40:2880-2888
57. **Uzarski RL, Pestka JJ** 2003 Comparative susceptibility of B cells with different lineages to cytotoxicity and apoptosis induction by translational inhibitors. J Toxicol Environ Health A 66:2105-2118
58. **Huynh HT, Robitaille G, Turner JD** 1991 Establishment of bovine mammary epithelial cells (MAC-T): an in vitro model for bovine lactation. Exp Cell Res 197:191-199
59. **Parikh BA, Coetzer C, Tumer NE** 2002 Pokeweed antiviral protein regulates the stability of its own mRNA by a mechanism that requires depurination but can be separated from depurination of the alpha-sarcin/ricin loop of rRNA. J Biol Chem 277:41428-41437
60. **Leibowitz BJ, Cohick WS** 2009 Endogenous IGFBP-3 is required for both growth factor-stimulated cell proliferation and cytokine-induced apoptosis in mammary epithelial cells. J Cell Physiol 220:182-188

61. **Wang HB, Xia F, Ge J, Yin J, Tan LS, Zhang PD, Zhong J** 2007 Co-application of ricin A chain and a recombinant adenovirus expressing ricin B chain as a novel approach for cancer therapy. Acta Pharmacol Sin 28:657-662
62. **Sandvig K, Bergan J, Dyve AB, Skotland T, Torgersen ML** 2009 Endocytosis and retrograde transport of Shiga toxin. Toxicon
63. **Vago R, Marsden CJ, Lord JM, Ippoliti R, Flavell DJ, Flavell SU, Ceriotti A, Fabbrini MS** 2005 Saporin and ricin A chain follow different intracellular routes to enter the cytosol of intoxicated cells. Febs J 272:4983-4995
64. **Wales R, Roberts LM, Lord JM** 1993 Addition of an endoplasmic reticulum retrieval sequence to ricin A chain significantly increases its cytotoxicity to mammalian cells. J Biol Chem 268:23986-23990
65. **Svinth M, Steighardt J, Hernandez R, Suh JK, Kelly C, Day P, Lord M, Girbes T, Robertus JD** 1998 Differences in cytotoxicity of native and engineered RIPs can be used to assess their ability to reach the cytoplasm. Biochem Biophys Res Commun 249:637-642
66. **Simmons BM, Stahl PD, Russell JH** 1986 Mannose receptor-mediated uptake of ricin toxin and ricin A chain by macrophages. Multiple intracellular pathways for a chain translocation. J Biol Chem 261:7912-7920
67. **Gray JS, Bae HK, Li JC, Lau AS, Pestka JJ** 2008 Double-stranded RNA-activated protein kinase mediates induction of interleukin-8 expression by deoxynivalenol, Shiga toxin 1, and ricin in monocytes. Toxicol Sci 105:322-330
68. **Wong J, Korcheva V, Jacoby DB, Magun BE** 2007 Proinflammatory responses of human airway cells to ricin involve stress-activated protein kinases and NF-kappaB. Am J Physiol Lung Cell Mol Physiol 293:L1385-1394
69. **Smallshaw JE, Richardson JA, Vitetta ES** 2007 RiVax, a recombinant ricin subunit vaccine, protects mice against ricin delivered by gavage or aerosol. Vaccine 25:7459-7469
70. **Bower JR, Congeni BL, Cleary TG, Stone RT, Wanger A, Murray BE, Mathewson JJ, Pickering LK** 1989 Escherichia coli O114:nonmotile as a pathogen in an outbreak of severe diarrhea associated with a day care center. J Infect Dis 160:243-247
71. **Karmali MA** 1989 Infection by verocytotoxin-producing Escherichia coli. Clin Microbiol Rev 2:15-38
72. **Lea N, Lord JM, Roberts LM** 1999 Proteolytic cleavage of the A subunit is essential for maximal cytotoxicity of Escherichia coli O157:H7 Shiga-like toxin-1. Microbiology 145 (Pt 5):999-1004

73. **Cherla RP, Lee SY, Tesh VL** 2003 Shiga toxins and apoptosis. FEMS Microbiol Lett 228:159-166
74. **Ogasawara T, Ito K, Igarashi K, Yutsudo T, Nakabayashi N, Takeda Y** 1988 Inhibition of protein synthesis by a Vero toxin (VT2 or Shiga-like toxin II) produced by Escherichia coli O157:H7 at the level of elongation factor 1-dependent aminoacyl-tRNA binding to ribosomes. Microb Pathog 4:127-135
75. **Hudak KA, Dinman JD, Tumer NE** 1999 Pokeweed antiviral protein accesses ribosomes by binding to L3. J Biol Chem 274:3859-3864
76. **Di R, Tumer NE** 2005 Expression of a truncated form of ribosomal protein L3 confers resistance to pokeweed antiviral protein and the Fusarium mycotoxin deoxynivalenol. Mol Plant Microbe Interact 18:762-770
77. **Jackson MP, Newland JW, Holmes RK, O'Brien AD** 1987 Nucleotide sequence analysis of the structural genes for Shiga-like toxin I encoded by bacteriophage 933J from Escherichia coli. Microb Pathog 2:147-153
78. **Fujii J, Matsui T, Heatherly DP, Schlegel KH, Lobo PI, Yutsudo T, Ciraolo GM, Morris RE, Obrig T** 2003 Rapid apoptosis induced by Shiga toxin in HeLa cells. Infect Immun 71:2724-2735
79. **Ikeda M, Gunji Y, Sonoda H, Oshikawa S, Shimono M, Horie A, Ito K, Yamasaki S** 2006 Inhibitory effect of tyrphostin 47 on Shiga toxin-induced cell death. Eur J Pharmacol 546:36-39
80. **Bouzari S, Oloomi M, Azadmanesh K** 2009 Study on induction of apoptosis on HeLa and Vero cells by recombinant shiga toxin and its subunits. Cytotechnology
81. **Jetzt AE, Cheng JS, Tumer NE, Cohick WS** 2009 Ricin A-chain requires c-Jun N-terminal kinase to induce apoptosis in nontransformed epithelial cells. Int J Biochem Cell Biol 41:2503-2510